

Supplementary Material for on-line publication only

Mechanistic Insights and Predictive Screening of M@C₂N

Catalysts for Urea Electrosynthesis from N₂ and CO₂

Nuttapon Yodsin^{a,*}, Tannatorn Potale^a, Yuwanda Injongkol^b,

Pimjai Pimbaotham^c, Supawadee Namuangruk^{d,*}

^a*Department of Chemistry, Faculty of Science, Silpakorn University, Nakhon Pathom 73000, Thailand*

^b*Futuristic Science Research Center, School of Science, Walailak University, Nakhonsrithammarat, 80160, Thailand.*

^c*Department of Chemistry and Center of Excellence for Innovation in Chemistry, Ubon Ratchathani University, Ubon Ratchathani, 34190, Thailand*

^d*National Nanotechnology Center (NANOTEC), National Science and Technology Development Agency (NSTDA), Pathum Thani 12120, Thailand.*

*Corresponding author. E-mail: yodsin_n@su.ac.th and supawadee@nanotec.or.th

Contents

Scheme S1 Proposed synthesis route for Fe-C₂N (Nb@C₂N, Mo@C₂N, and Re@C₂N)

Figure S1-3 – Stable optimized configurations of 3d-, 4d-, 5d-M@C₂N, respectively.

Table S1. Computed formation energy (E_f) and dissolution potential (U_{diss}) of metals, and number of transferred electrons (N_e) during the dissolution. The standard dissolution potentials ($U^\circ diss$) of metal atoms are also listed for comparison.

Figure S4-S6 – Stable optimized N₂ adsorption configurations of 3d-, 4d-, 5d-M@C₂N, respectively.

Figure S7-S16 – Atomic structures of critical step through the four possible pathways; the CO₂ pathway (ΔG_{*CO_2+*NNH}), OCOH pathway ($\Delta G_{*OCOH+*NNH}$), the CO pathway ($\Delta G_{*CO+*NNH}$), and the NCON pathway (ΔG_{*NCON}) on selected M@C₂N.

Figure S17-S25 – Gibbs free energy diagrams and atomic structures of critical step through the CO₂ pathways for urea formation on M@C₂N (M: Ti, V, Cr, Zr, Nb, Hf, Ta, W, and Re).

Figure S26-S30 – Gibbs free energy diagrams and atomic structures of critical step through the CO pathways for urea formation on M@C₂N (M: Ti, Mn, Mo, Hf, and W).

Figure S31-S35 – Gibbs free energy diagrams and atomic structures of critical step through the OCOH pathways for urea formation on M@C₂N (M: V, Cr, Nb, Ta, and Re).

Table S2 The limiting potential of urea production (U_L) on the screened M@C₂N surface (M; Ti, V, Cr, Mn, Nb, Mo, Ru, Hf, Ta, W, and Re).

Figure36 – The geometrical structures of (a.) Nb@C₂N, (b.) Mo@C₂N and (c.) Re@C₂N catalysts

Table R3 Gibbs free energy (G, eV) and Nb magnetization values (μ_B) of the intermediates in the $*CO_2+*N_2 \rightarrow *CO_2 + *NNH$ step on Nb@C₂N at different U values.

Table R4 Gibbs free energy (G, eV) and Mo magnetization values (μ_B) of the intermediates in the $*CO+*N_2 \rightarrow *CO + *NNH$ step on Mo@C₂N at different U values.

Table R5 Gibbs free energy (G, eV) and Re magnetization values (μ_B) of the intermediates in the $*CO_2+*N_2 \rightarrow *CO_2 + *NNH$ step on Re@C₂N at different U values.

Table R6 Gibbs free energy (G, eV) of the intermediates in the $*CO_2/CO+*N_2 \rightarrow *CO_2/CO + *NNH$ step on Nb@C₂N with and without VASPsol calculation.

Table S7. Specific values of different features included in the descriptor Φ .

Table S8. Specific values of different features included in the descriptor φ .

Table S9. Values of descriptor Φ and ΔG_L of PDS for urea production over reported electrocatalysts.

Figure37 – Gibbs free energy adsorption for H^+ , H_2O , and N_2 on $Nb@C_2N$, $Mo@C_2N$, and $Re@C_2N$ catalysts

Figure38 – Gibbs free energy diagrams and atomic structures of CRR on $Nb@C_2N$ catalysts

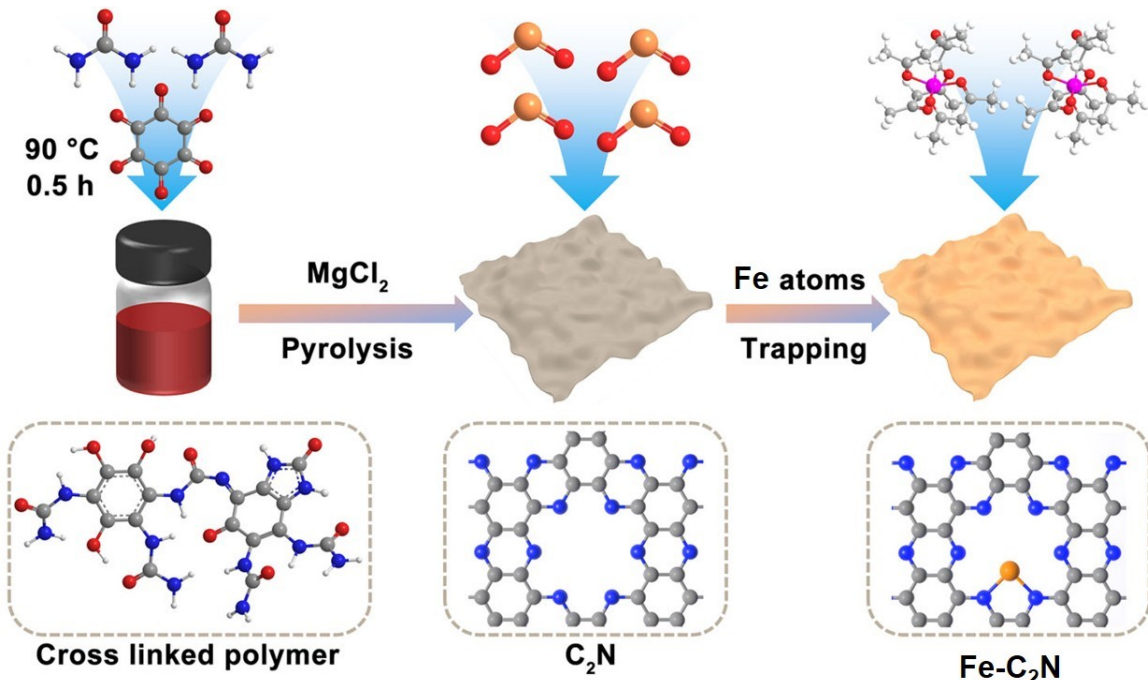
Figure39 – Gibbs free energy diagrams and atomic structures of NRR on $Nb@C_2N$ catalysts

Figure40 – Gibbs free energy diagrams and atomic structures of CRR on $Mo@C_2N$ catalysts

Figure41 – Gibbs free energy diagrams and atomic structures of NRR on $Mo@C_2N$ catalysts

Figure42 – Gibbs free energy diagrams and atomic structures of CRR on $Re@C_2N$ catalysts

Figure43 – Gibbs free energy diagrams and atomic structures of NRR on $Re@C_2N$ catalysts



Scheme S1. Proposed synthesis route for Fe-C₂N (Nb@C₂N, Mo@C₂N, and Re@C₂N)

The synthesis routes have been developed by Wang and co-workers¹ such as the thermal treatment of a mixture of cyclohexanehexone and urea, followed by calcination at various temperatures (500-1000 °C) in the presence of MgCl₂ under nitrogen atmosphere. The carbonized products are then purified and dried to yield C₂N materials with different crystallinities and surface properties. Details are below.

Preparation of C₂N

1. A well-ground mixture of cyclohexanehexone and urea was prepared in a molar ratio of 1:4.5.
2. This mixture was gently heated at 90 °C for 30 minutes.
3. The resulting cross-linked product was then mixed with anhydrous MgCl₂ in a mass ratio of 1:3.75 and ground thoroughly.
4. The mixture was calcined at 500, 800, 900, and 1000 °C for 2 hours, with a heating rate of 3 °C/min under a nitrogen atmosphere.
5. After cooling to room temperature, the carbonized samples were washed sequentially with 0.5 M sulfuric acid, deionized water, and ethanol.
6. Finally, the washed samples were dried overnight in a vacuum oven at 60 °C to yield C₂N-500, C₂N-800, C₂N-900, and C₂N-1000, respectively.

Preparation of Fe-C₂N

1. 90 mg of the prepared C₂N was mixed with 6 mg of iron (III) acetylacetone (Fe(acac)₃) using a simple grinding method.
2. The resulting powder was then placed in a tube furnace and heated to 900 °C at a rate of 3 °C per minute under a flowing nitrogen atmosphere.
3. Once the target temperature was reached, the material was annealed for 2 hours.
4. After naturally cooling to room temperature, the final product, Fe-C₂N, was obtained and used directly without any further treatment.

Although the direct synthesis of Nb@C₂N, Mo@C₂N, and Re@C₂N has not yet been documented in the literature, we propose that it is achievable by substituting the commonly used iron precursor, such as iron (III) acetylacetone, with suitable alternatives. These include niobium oxalate (C₁₀H₅NbO₂₀)² or niobium pentachloride (NbCl₅)³ for Nb, molybdenum(V) chloride (MoCl₅)⁴ for Mo, and ammonium perrhenate (NH₄ReO₄)⁵ for Re, enabling the synthesis of single-atom catalysts based on each metal.

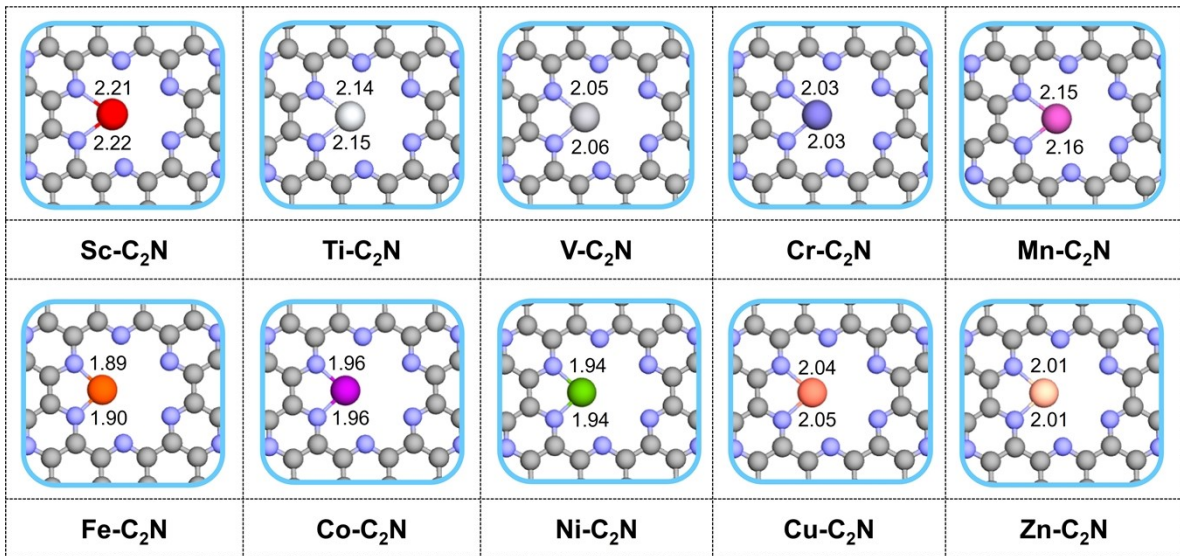


Figure S1 – Stable optimized configurations of 3d–M@C₂N

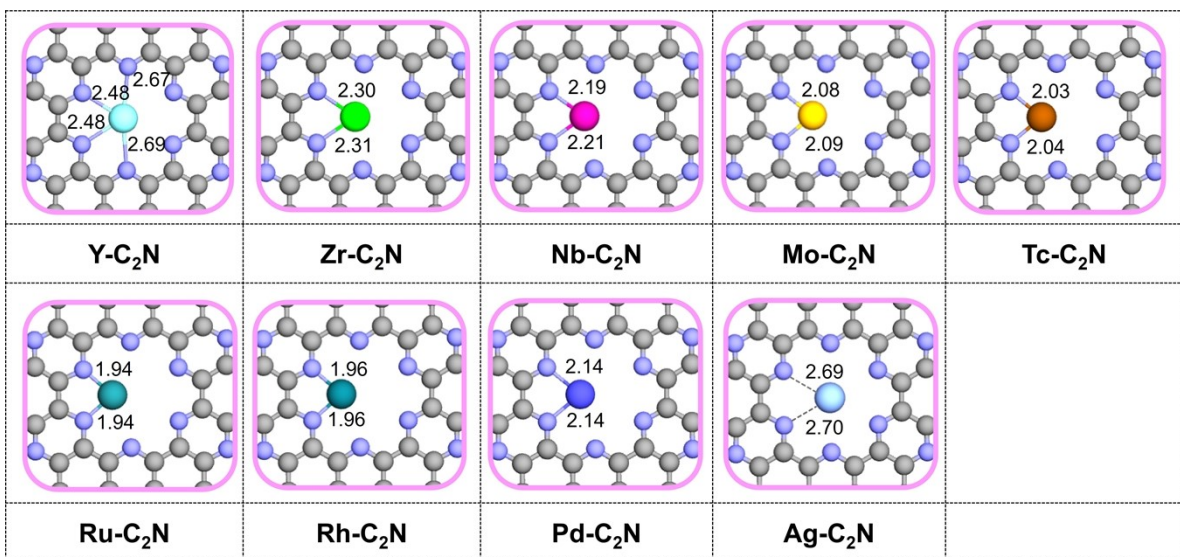


Figure S2 – Stable optimized configurations of 4d–M@C₂N

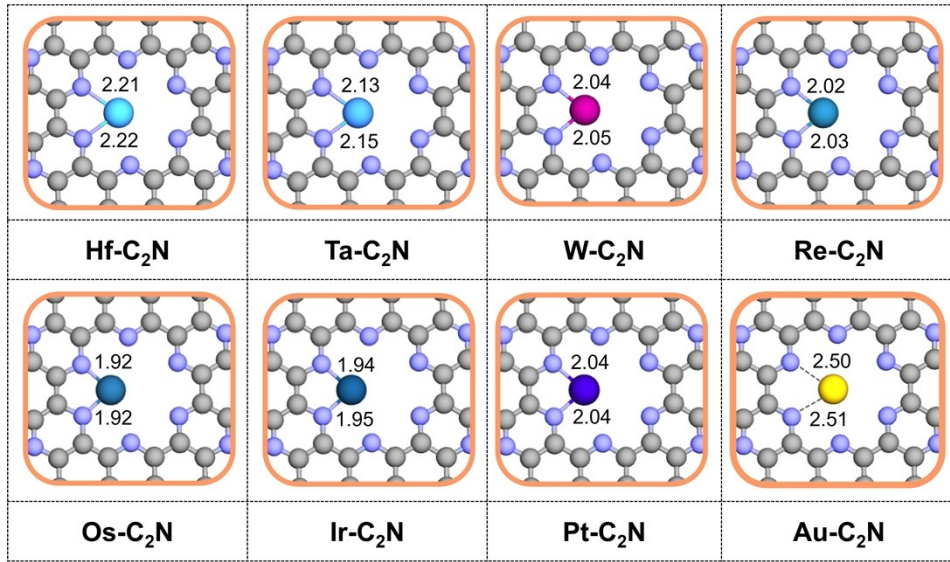


Figure S3 – Stable optimized configurations of 5d–M@C₂N

Table S1. Computed formation energy (E_f) and dissolution potential (U_{diss}) of metals, and number of transferred electrons (N_e) during the dissolution. The standard dissolution potentials ($U^\circ diss$) of metal atoms are also listed for comparison.

Metal	N_e	$U^\circ diss$ (V)	E_f (eV)	U_{diss} (V)
Sc	3	-2.08	-7.56	0.44
Ti	2	-1.63	-6.98	1.86
V	2	-1.18	-6.02	1.83
Cr	2	-0.91	-4.46	1.32
Mn	2	-1.19	-4.36	0.26
Fe	2	-0.45	-4.27	1.69
Co	2	-0.28	-5.07	2.26
Ni	2	-0.26	-4.87	2.17
Cu	2	0.34	-3.31	2.00
Zn	2	-0.76	-1.39	-0.06
Y	3	-2.37	-8.60	0.50
Zr	4	-1.45	-8.57	0.69

Nb	3	-1.10	-7.27	1.32
Mo	3	-0.20	-5.32	1.57
Ru	2	0.46	-6.65	3.78
Rh	2	0.60	-5.34	3.27
Pd	2	0.95	-3.30	4.25
Ag	1	0.80	-2.92	3.72
Hf	4	-1.55	-8.30	0.52
Ta	3	-0.60	-7.80	2.00
W	3	0.10	-6.57	2.29
Re	3	0.30	-4.98	1.96
Os	8	0.84	-5.87	1.57
Ir	3	1.16	-5.75	3.08
Pt	2	1.18	-4.19	3.27
Au	3	1.50	-2.22	2.24

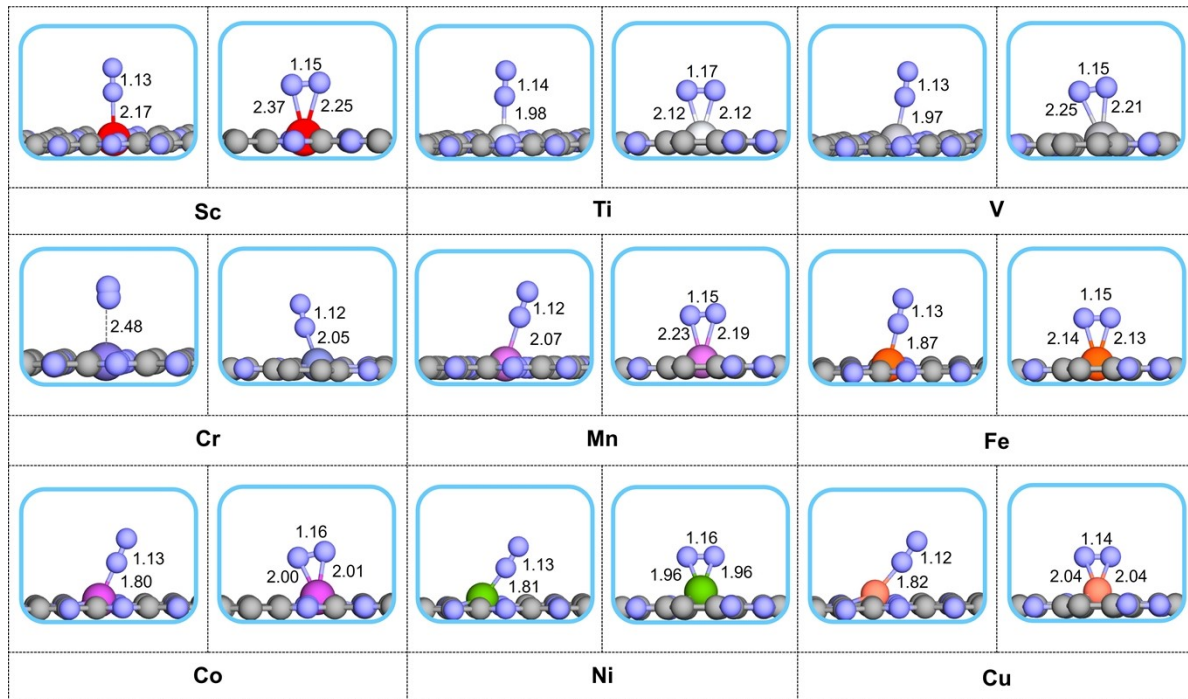


Figure S4 – Stable optimized N_2 adsorption configurations of $3d\text{-M@C}_2\text{N}$

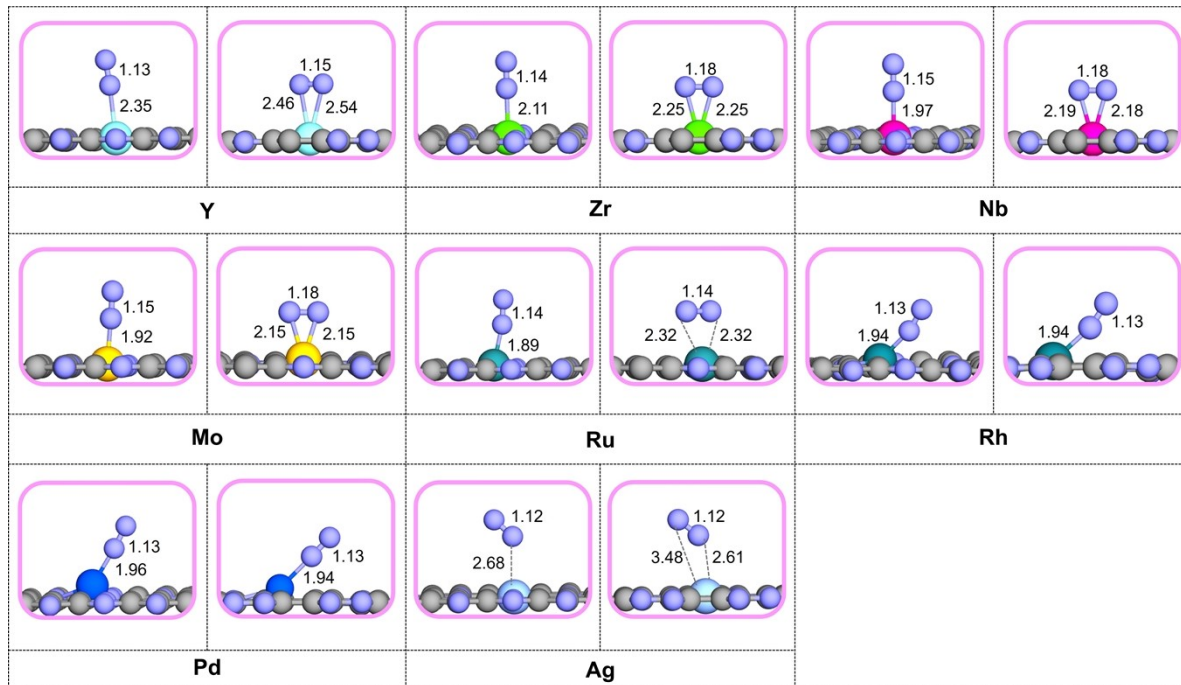


Figure S5 – Stable optimized N₂ adsorption configurations of 4d–M@C₂N

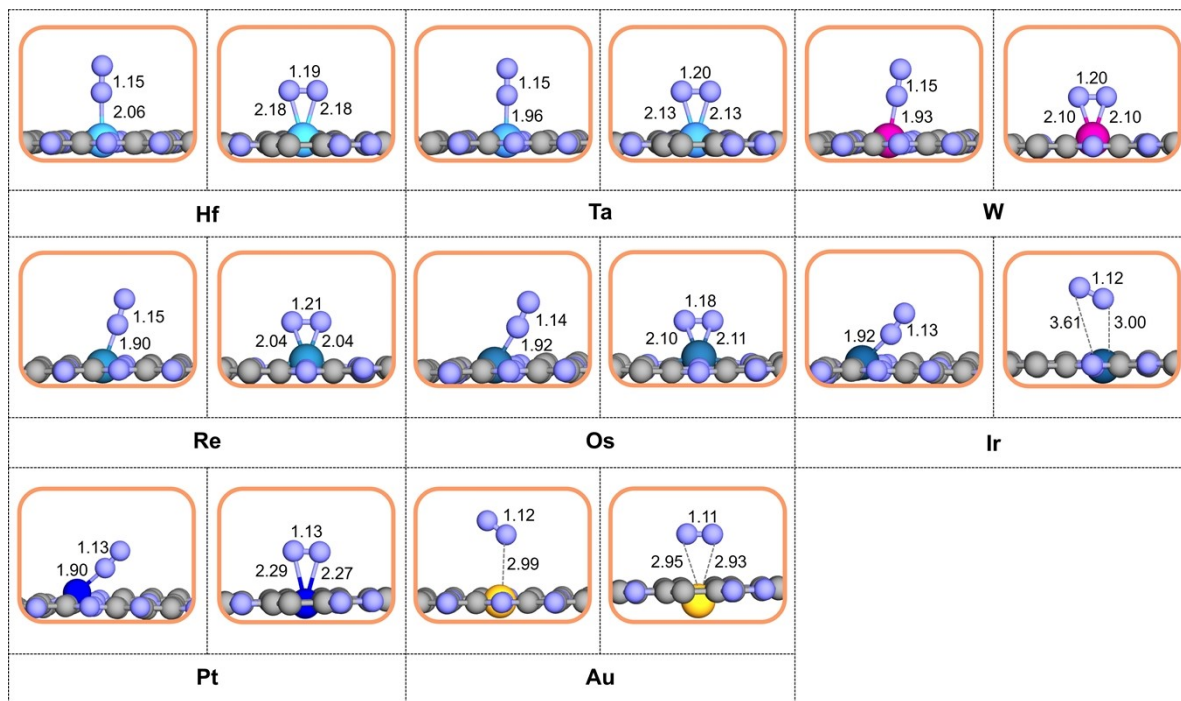


Figure S6 – Stable optimized N₂ adsorption configurations of 5d–M@C₂N

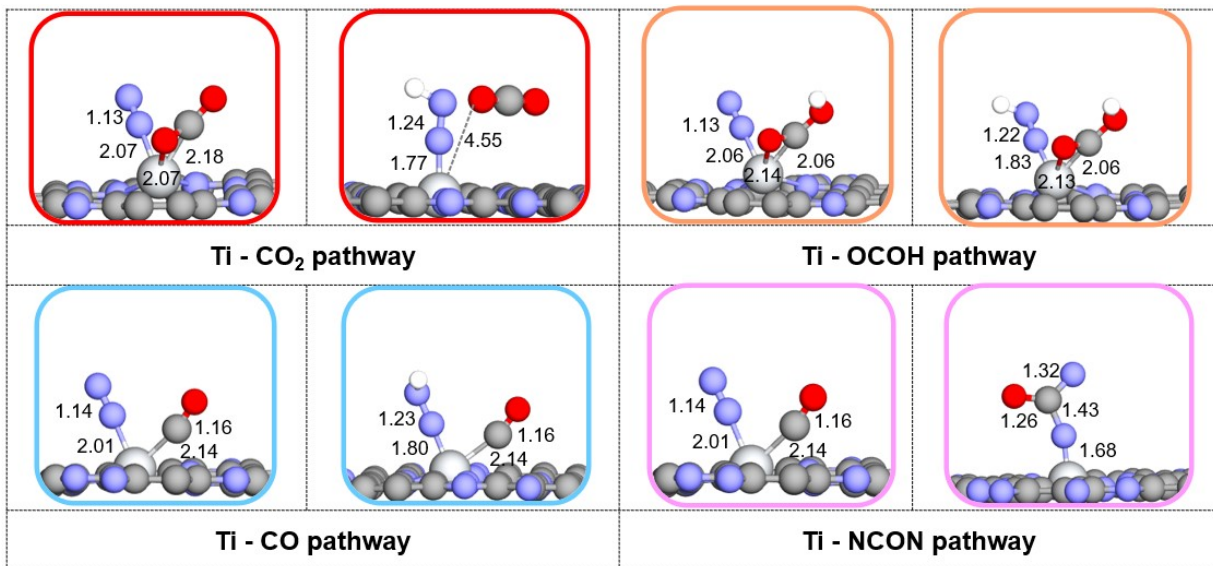


Figure S7 – Atomic structures of critical step through the four possible pathways; the CO₂ pathway ($\Delta G^*_{\text{CO}_2+\text{*NNH}}$), OCOH pathway ($\Delta G^*_{\text{OCOH}+\text{*NNH}}$), the CO pathway ($\Delta G^*_{\text{CO}+\text{*NNH}}$), and the NCON pathway (ΔG^*_{NCON}) on Ti@C₂N.

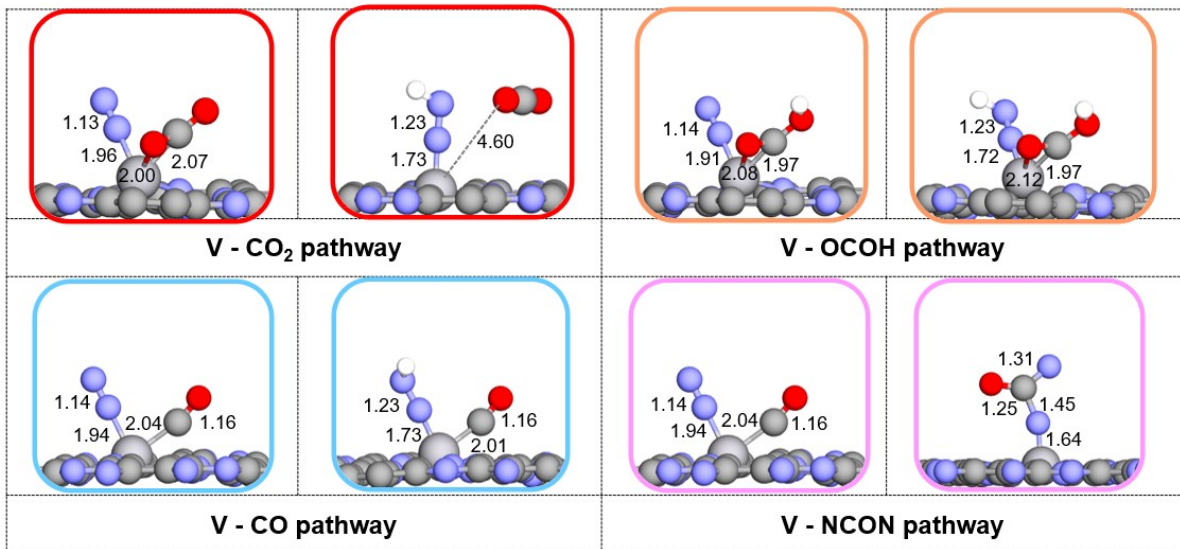


Figure S8 – Atomic structures of critical step through the four possible pathways; the CO₂ pathway ($\Delta G^*_{\text{CO}_2+\text{*NNH}}$), OCOH pathway ($\Delta G^*_{\text{OCOH}+\text{*NNH}}$), the CO pathway ($\Delta G^*_{\text{CO}+\text{*NNH}}$), and the NCON pathway (ΔG^*_{NCON}) on V@C₂N.

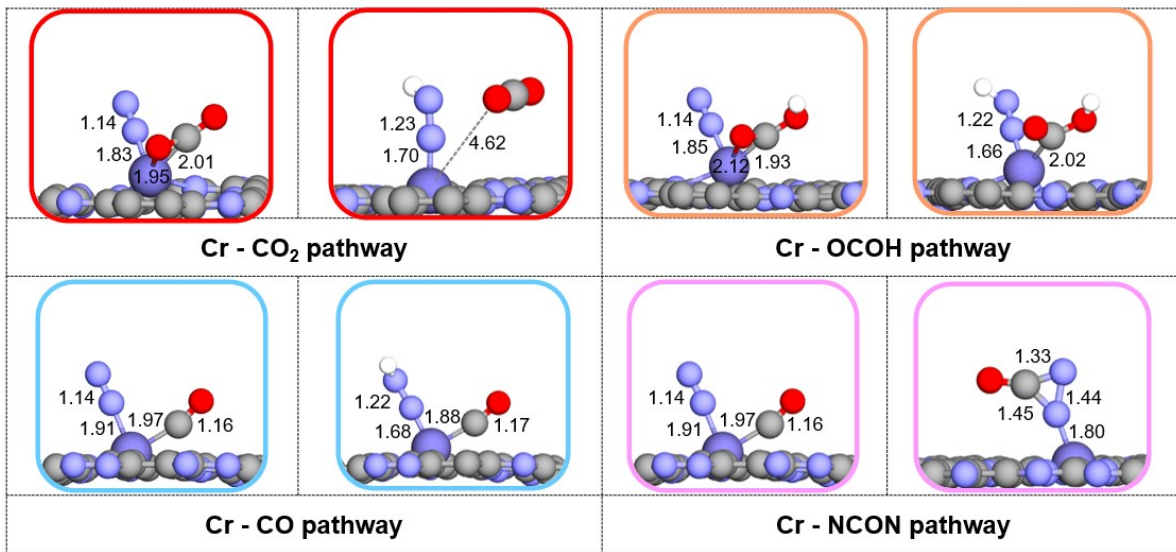


Figure S9 – Atomic structures of critical step through the four possible pathways; the CO₂ pathway (ΔG_{*CO_2+*NNH}), OCOH pathway ($\Delta G_{*OCOH+*NNH}$), the CO pathway ($\Delta G_{*CO+*NNH}$), and the NCON pathway (ΔG_{*NCON}) on Cr@C₂N.

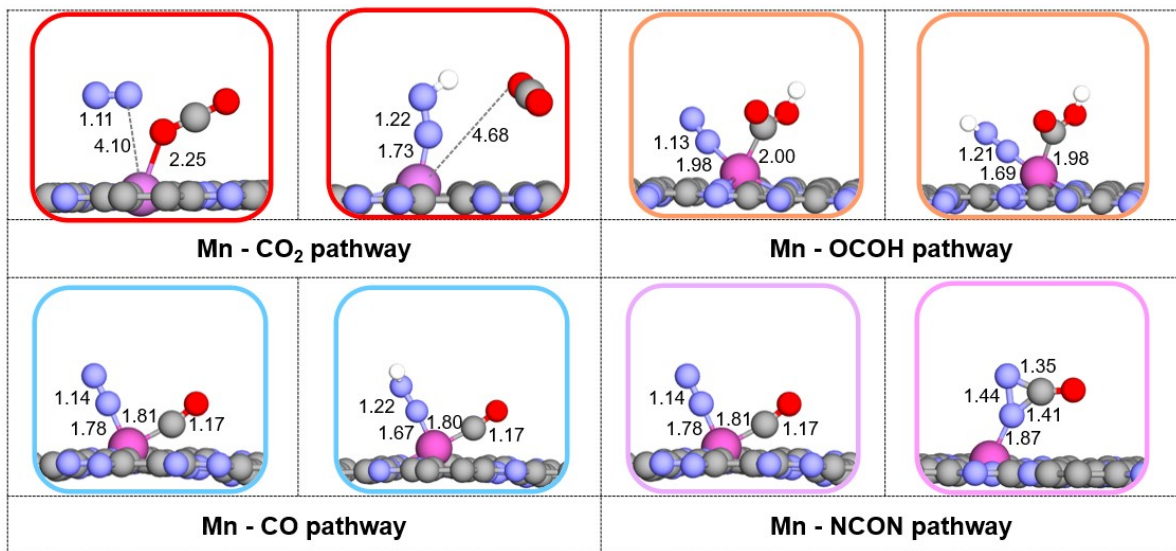


Figure S10 – Atomic structures of critical step through the four possible pathways; the CO₂ pathway (ΔG_{*CO_2+*NNH}), OCOH pathway ($\Delta G_{*OCOH+*NNH}$), the CO pathway ($\Delta G_{*CO+*NNH}$), and the NCON pathway (ΔG_{*NCON}) on Mn@C₂N.

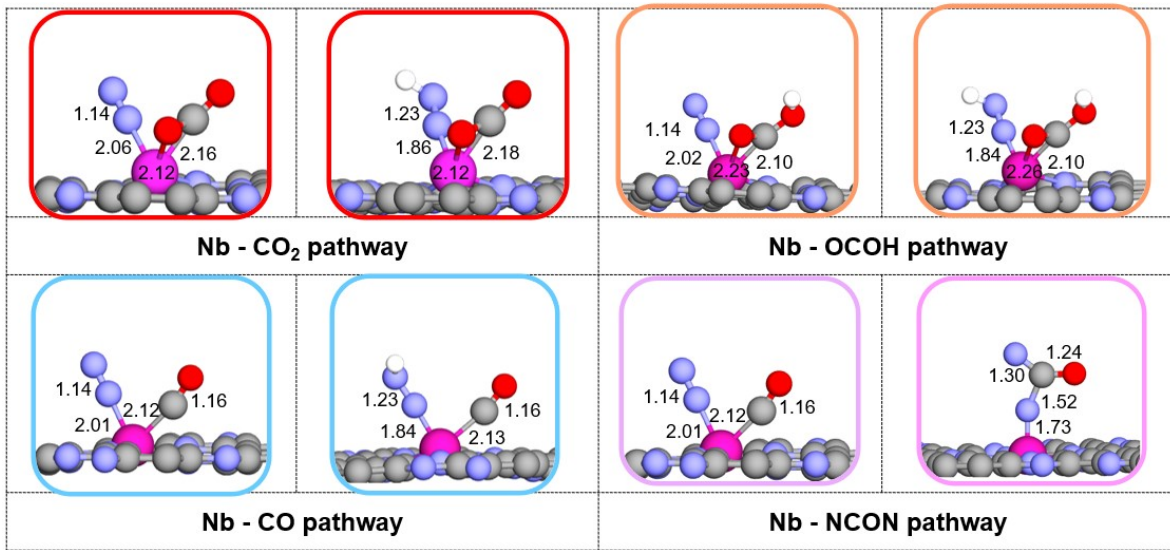


Figure S11 – Atomic structures of critical step through the four possible pathways; the CO₂ pathway ($\Delta G^*_{\text{CO}_2+\text{*NNH}}$), OCOH pathway ($\Delta G^*_{\text{OCOH}+\text{*NNH}}$), the CO pathway ($\Delta G^*_{\text{CO}+\text{*NNH}}$), and the NCON pathway (ΔG^*_{NCON}) on Nb@C₂N.

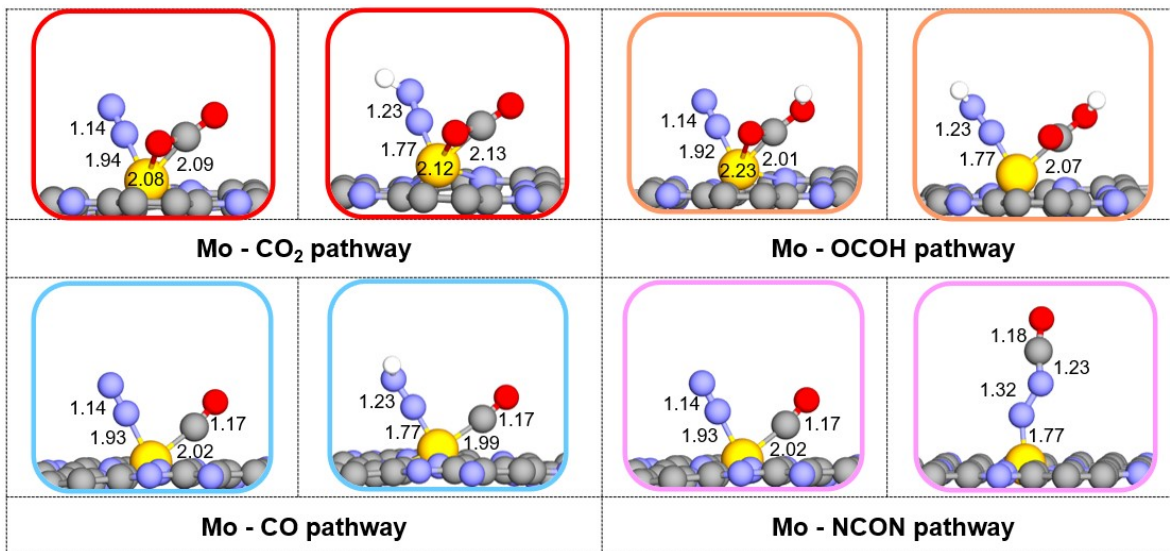


Figure S12 – Atomic structures of critical step through the four possible pathways; the CO₂ pathway ($\Delta G^*_{\text{CO}_2+\text{*NNH}}$), OCOH pathway ($\Delta G^*_{\text{OCOH}+\text{*NNH}}$), the CO pathway ($\Delta G^*_{\text{CO}+\text{*NNH}}$), and the NCON pathway (ΔG^*_{NCON}) on Mo@C₂N.

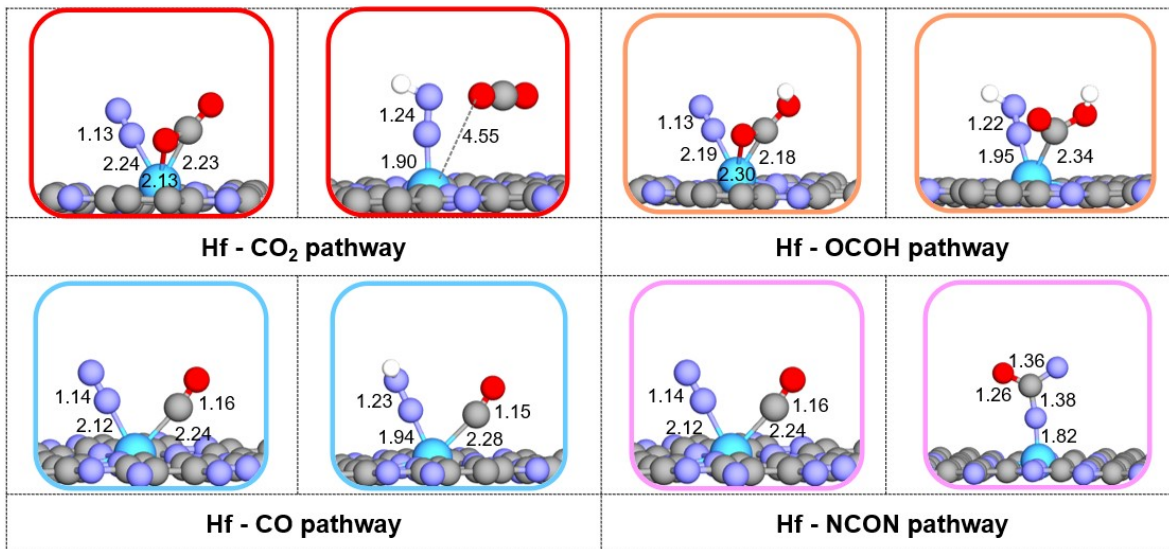


Figure S13 – Atomic structures of critical step through the four possible pathways; the CO₂ pathway (ΔG_{*CO_2+*NNH}), OCOH pathway ($\Delta G_{*OCOH+*NNH}$), the CO pathway ($\Delta G_{*CO+*NNH}$), and the NCON pathway (ΔG_{*NCON}) on Hf@C₂N.

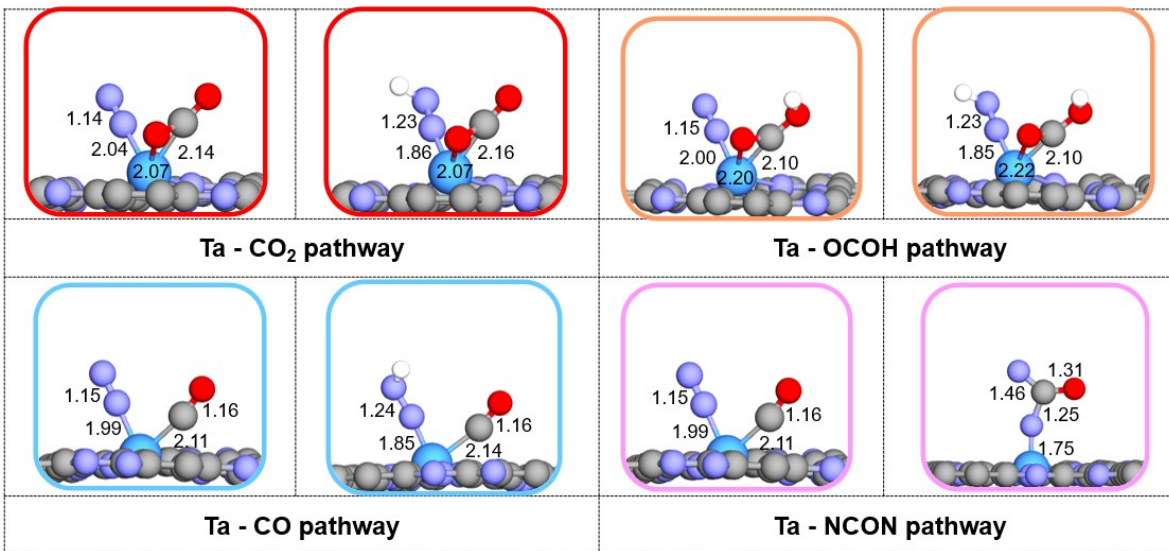


Figure S14 – Atomic structures of critical step through the four possible pathways; the CO₂ pathway (ΔG_{*CO_2+*NNH}), OCOH pathway ($\Delta G_{*OCOH+*NNH}$), the CO pathway ($\Delta G_{*CO+*NNH}$), and the NCON pathway (ΔG_{*NCON}) on Ta@C₂N.

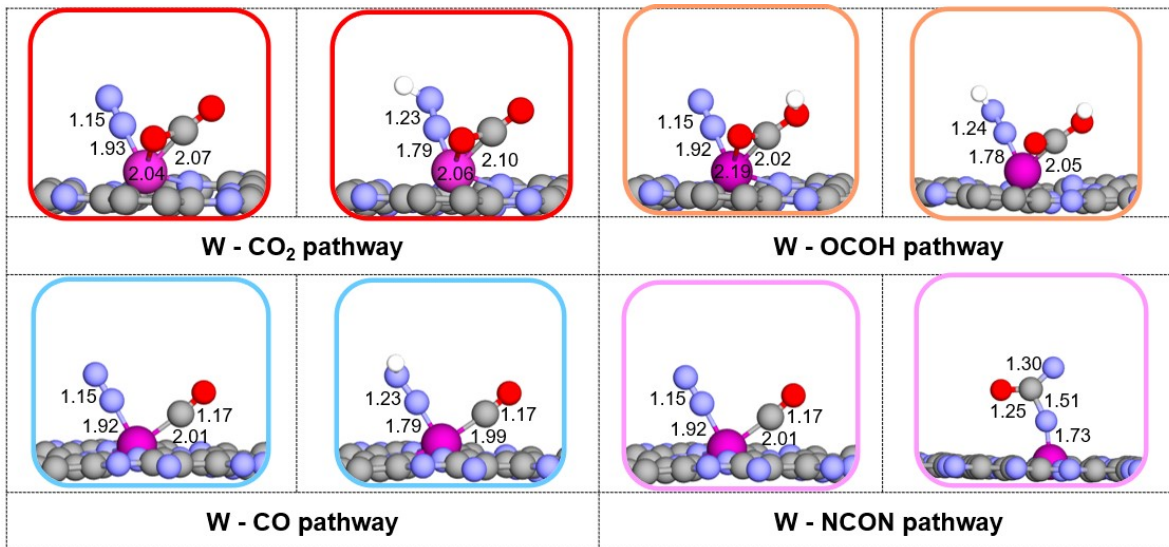


Figure S15 – Atomic structures of critical step through the four possible pathways; the CO₂ pathway ($\Delta G^*_{\text{CO}_2+\text{*NNH}}$), OCOH pathway ($\Delta G^*_{\text{OCOH}+\text{*NNH}}$), the CO pathway ($\Delta G^*_{\text{CO}+\text{*NNH}}$), and the NCON pathway (ΔG^*_{NCON}) on W@C₂N.

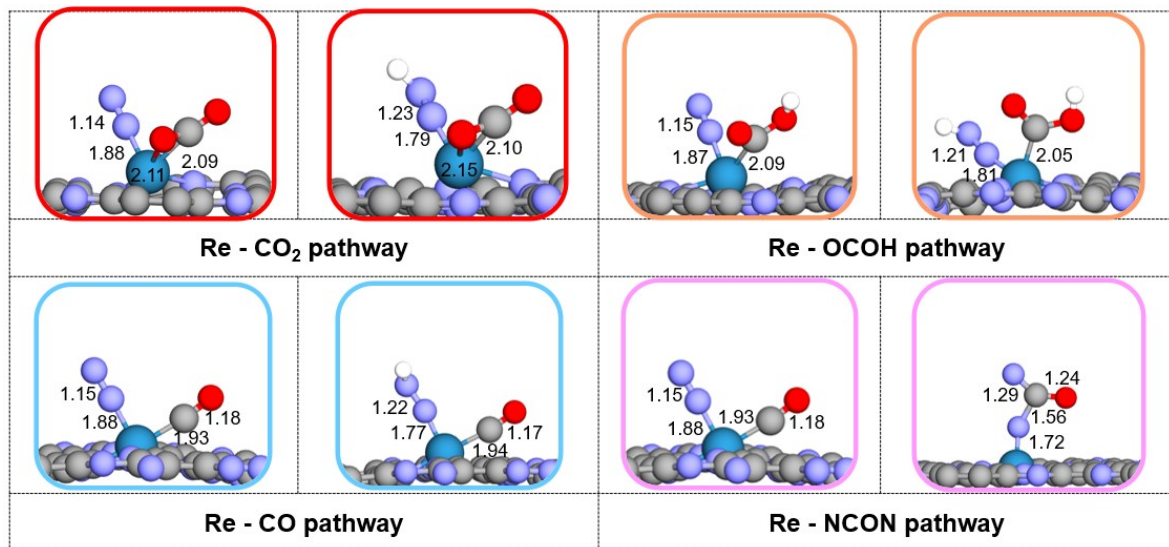


Figure S16 – Atomic structures of critical step through the four possible pathways; the CO₂ pathway ($\Delta G^*_{\text{CO}_2+\text{*NNH}}$), OCOH pathway ($\Delta G^*_{\text{OCOH}+\text{*NNH}}$), the CO pathway ($\Delta G^*_{\text{CO}+\text{*NNH}}$), and the NCON pathway (ΔG^*_{NCON}) on Re@C₂N.

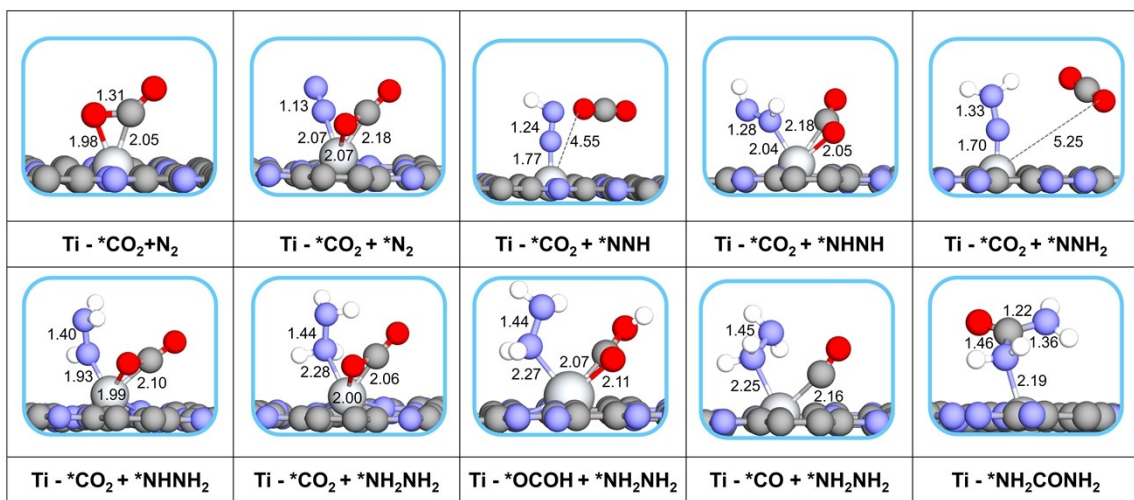
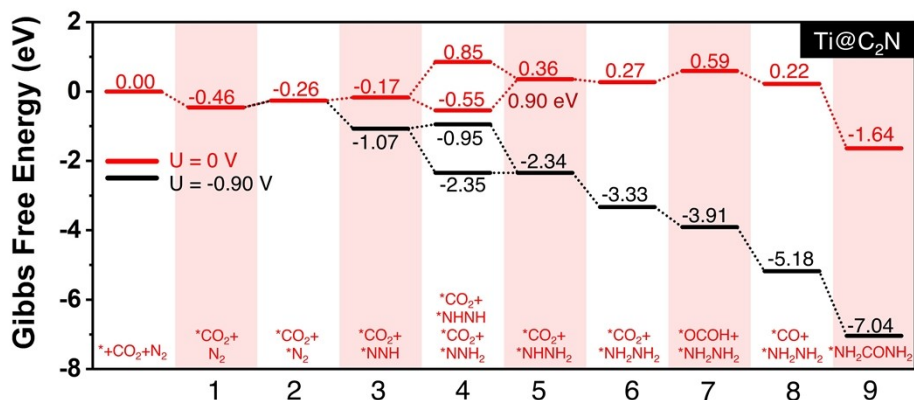


Figure S17 – Gibbs free energy diagrams and atomic structures of critical step through the CO₂ pathways for urea formation on Ti@C₂N.

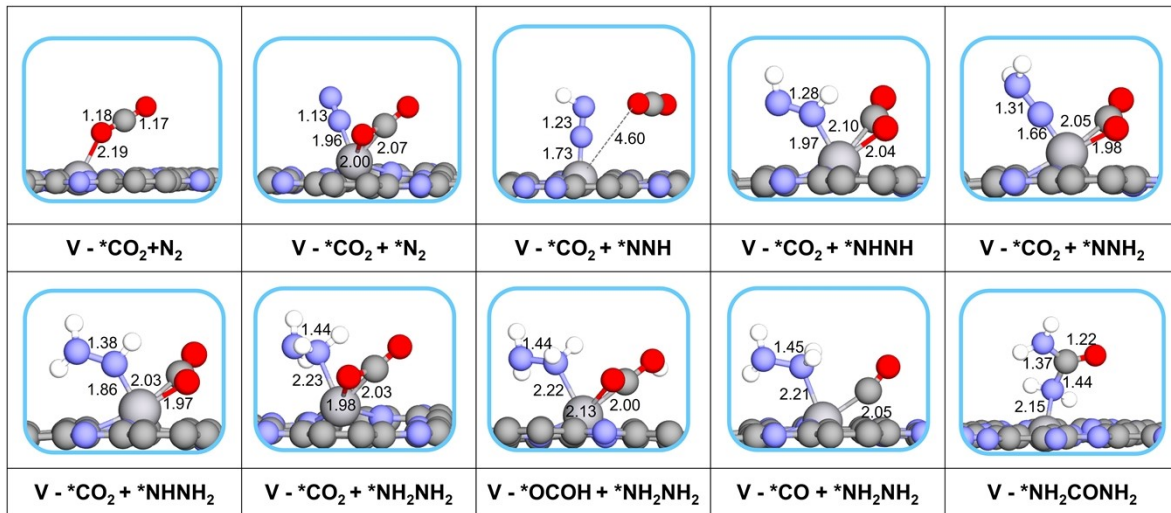
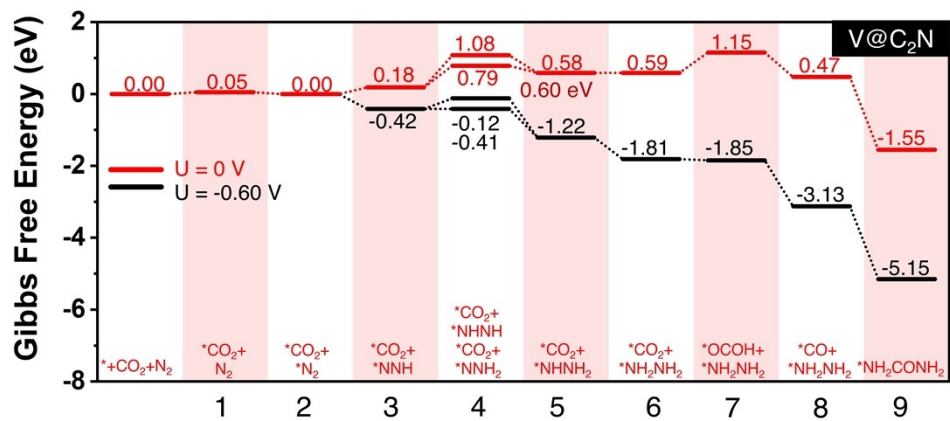


Figure S18 – Gibbs free energy diagrams and atomic structures of critical step through the CO₂ pathways for urea formation on V@C₂N.

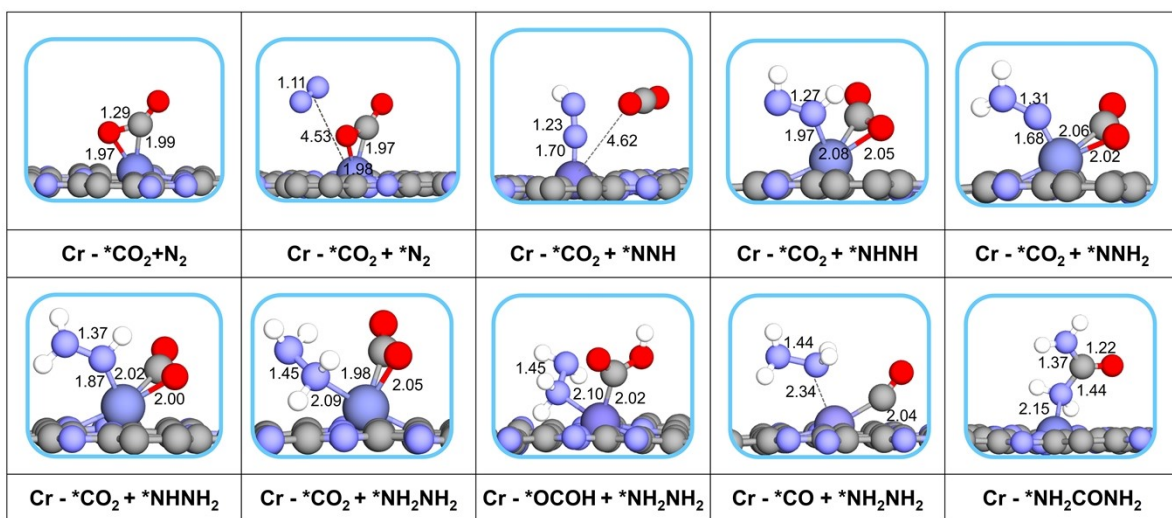
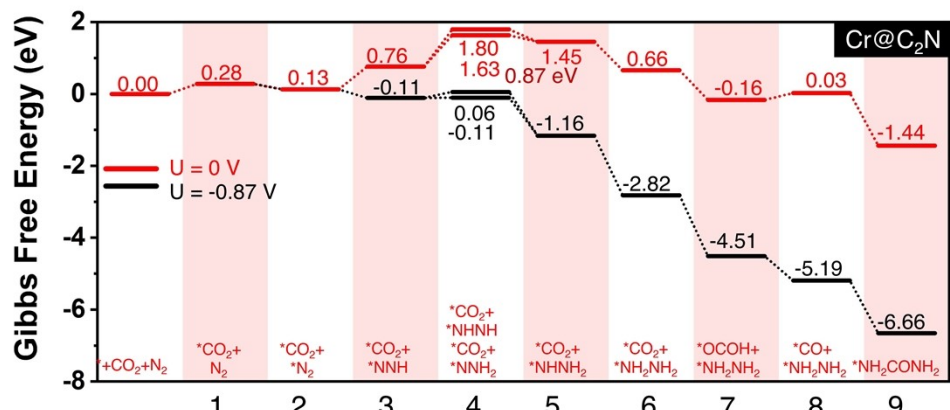


Figure S19 – Gibbs free energy diagrams and atomic structures of critical step through the CO₂ pathways for urea formation on Cr@C₂N.

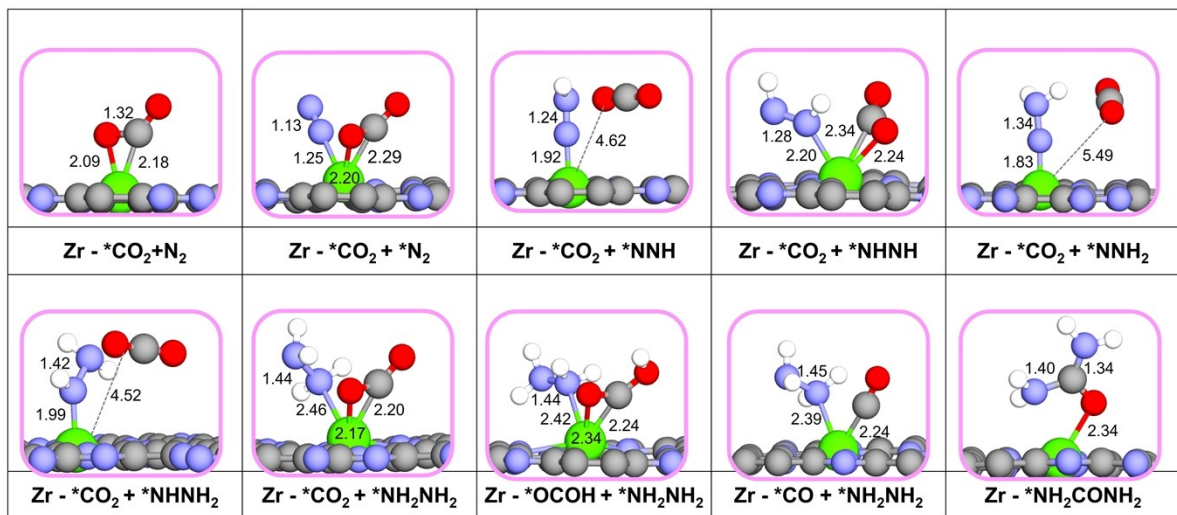
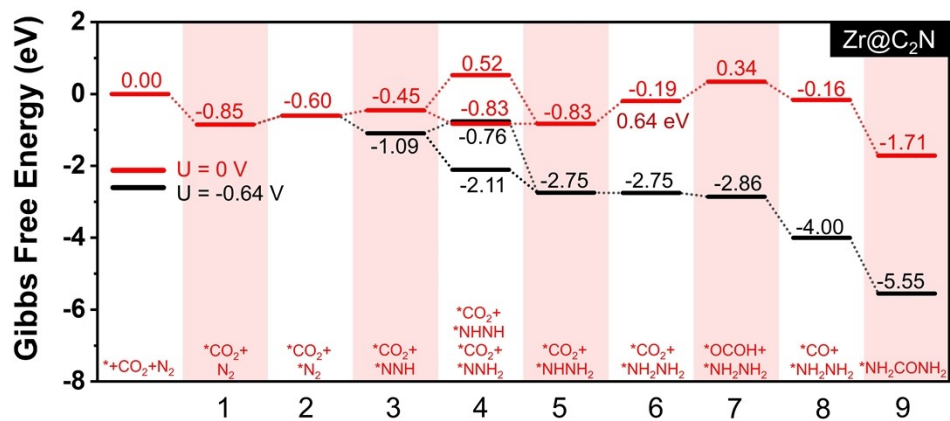


Figure S20 – Gibbs free energy diagrams and atomic structures of critical step through the CO_2 pathways for urea formation on $\text{Zr}@\text{C}_2\text{N}$.

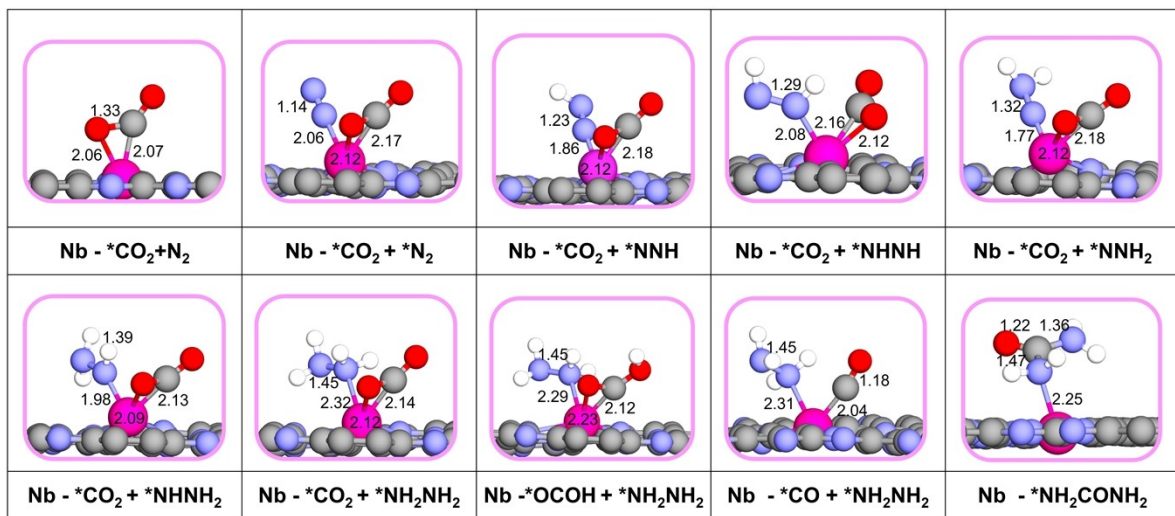
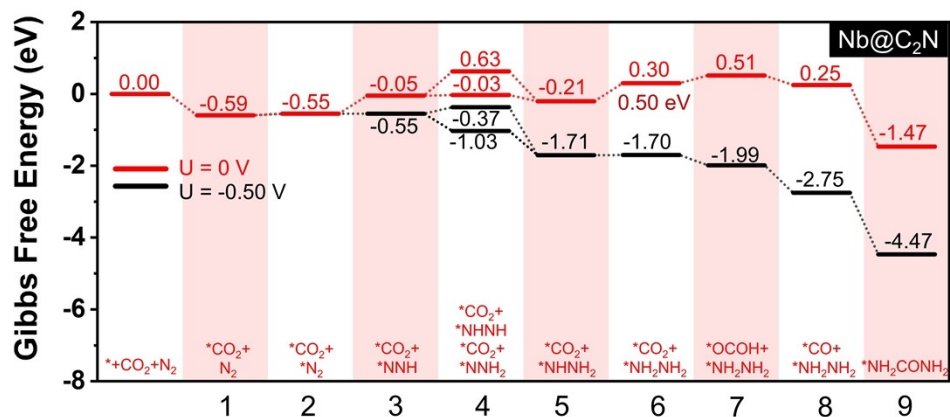


Figure S21 – Gibbs free energy diagrams and atomic structures of critical step through the CO₂ pathways for urea formation on Nb@C₂N.

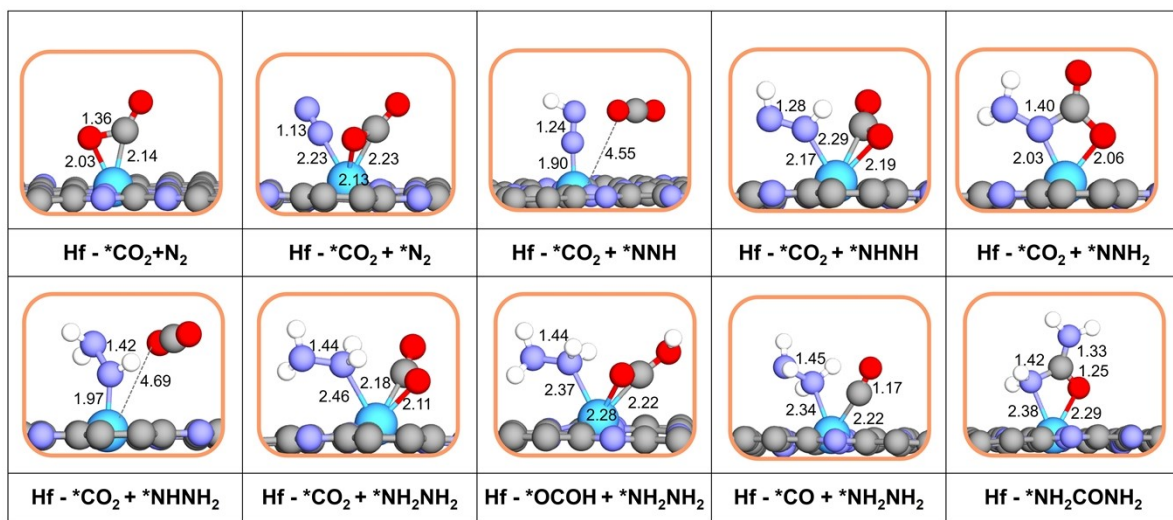
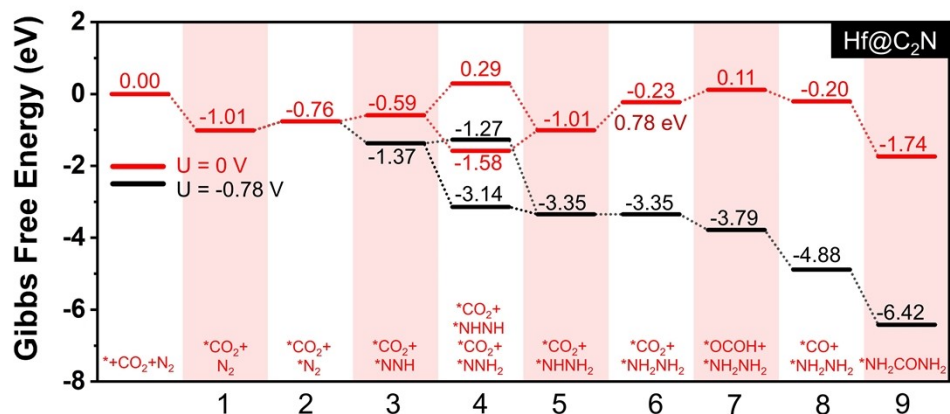


Figure S22 – Gibbs free energy diagrams and atomic structures of critical step through the CO_2 pathways for urea formation on $\text{Hf}@\text{C}_2\text{N}$.

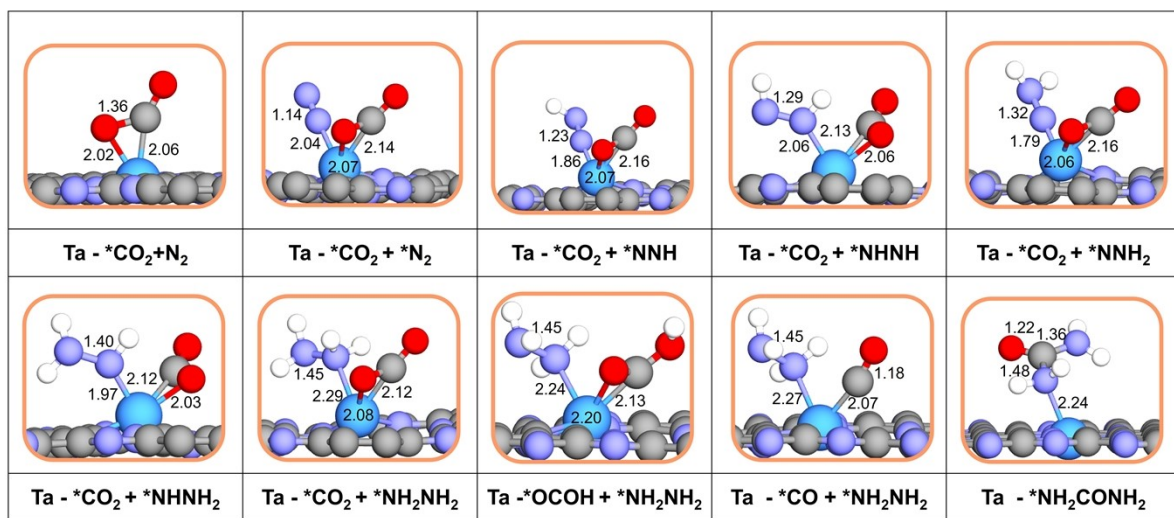
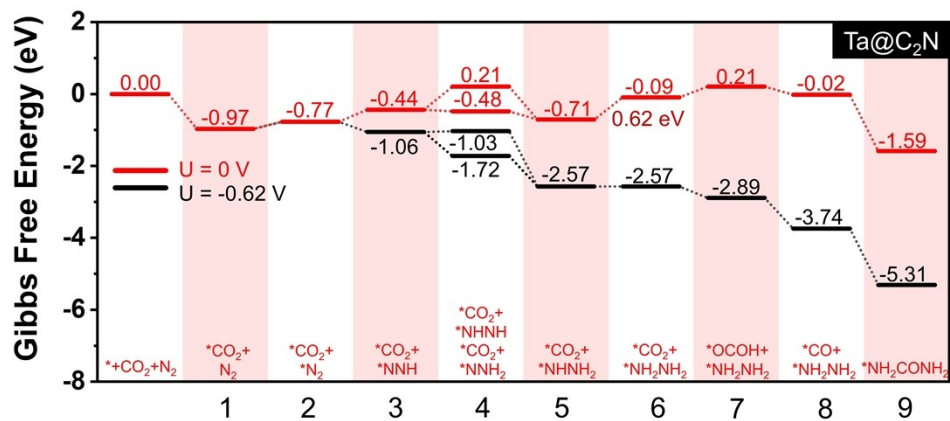


Figure S23 – Gibbs free energy diagrams and atomic structures of critical step through the CO₂ pathways for urea formation on Ta@C₂N.

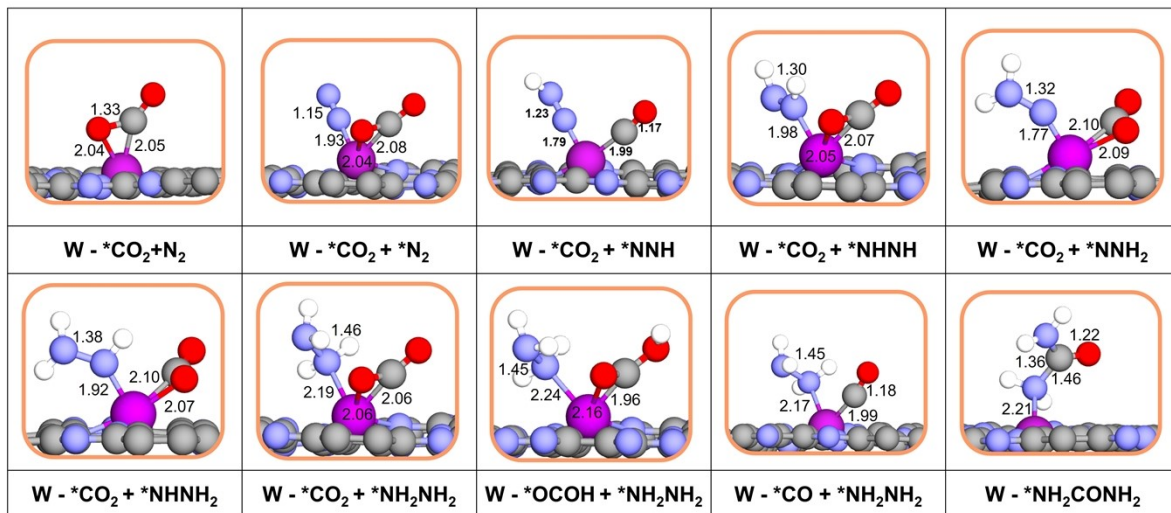
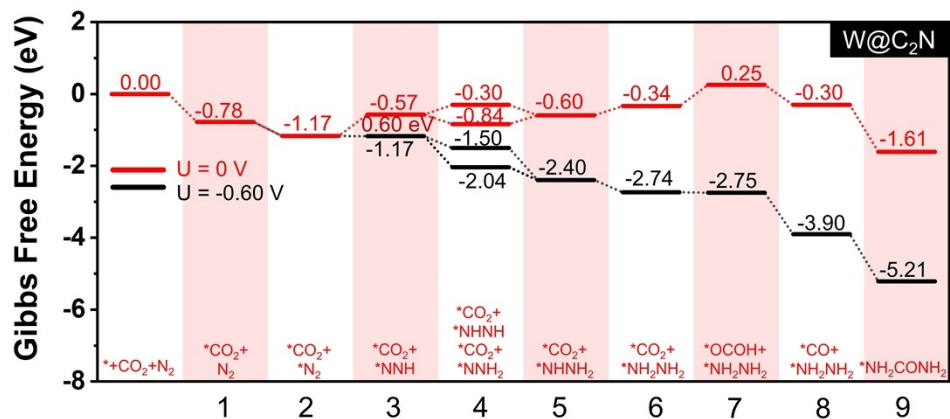


Figure S24 – Gibbs free energy diagrams and atomic structures of critical step through the CO₂ pathways for urea formation on W@C₂N.

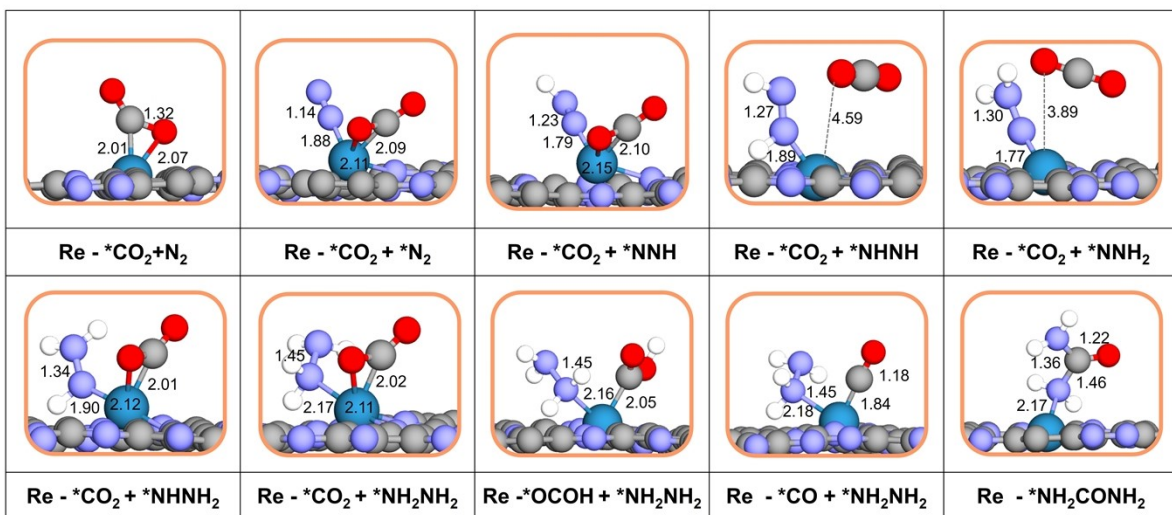
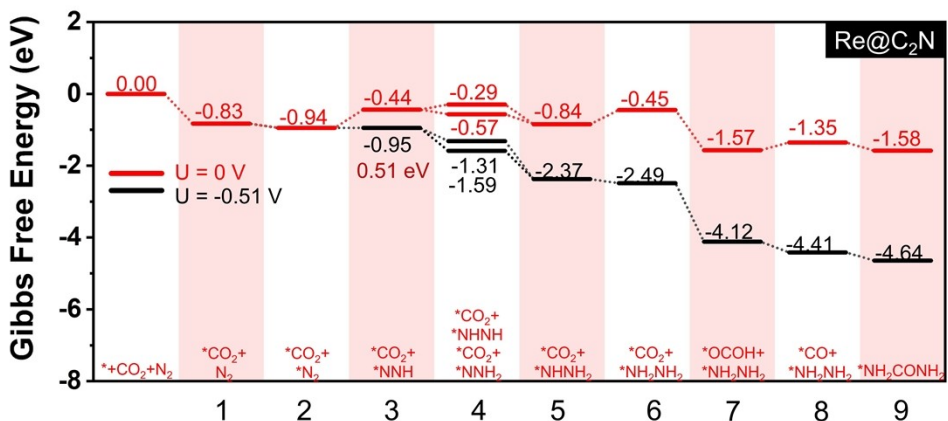


Figure S25 – Gibbs free energy diagrams and atomic structures of critical step through the CO₂ pathways for urea formation on Re@C₂N.

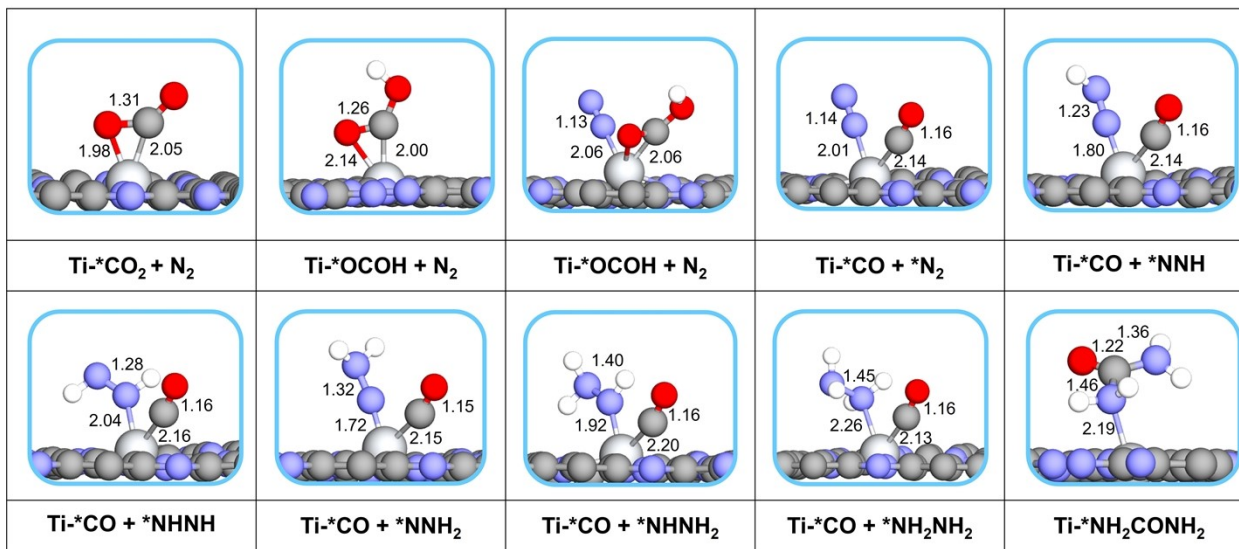
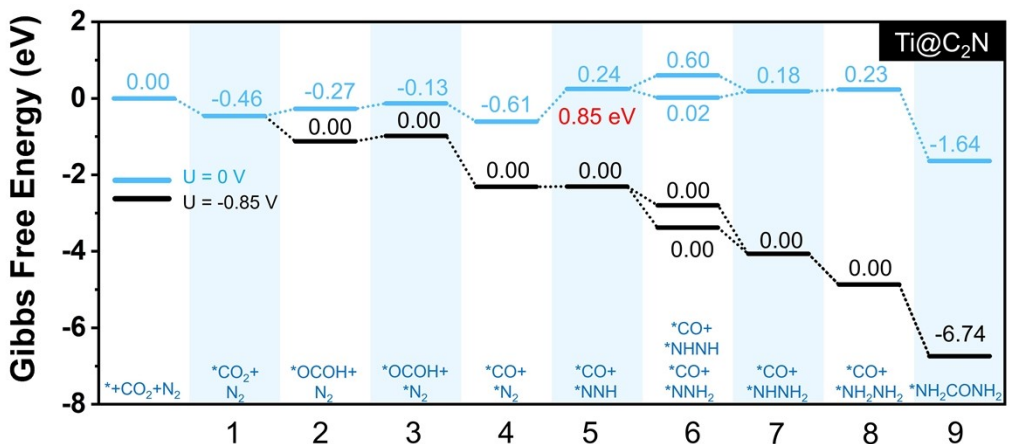


Figure S26 – Gibbs free energy diagrams and atomic structures of critical step through the CO pathways for urea formation on Ti@C₂N.

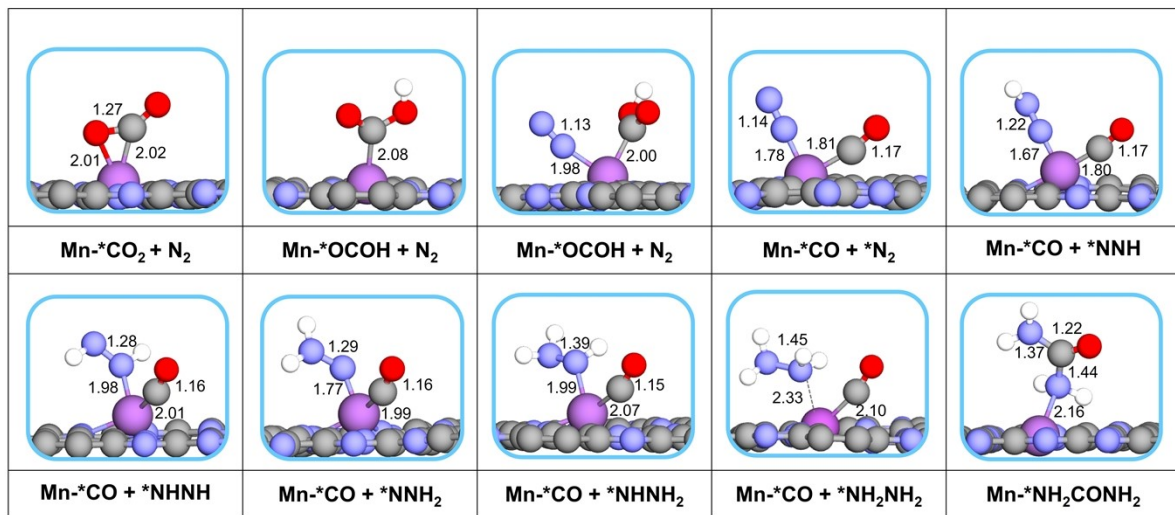
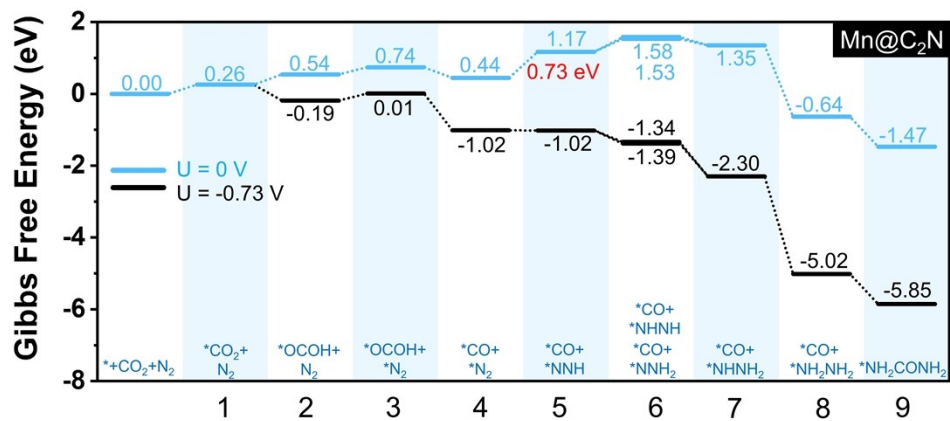


Figure S27 – Gibbs free energy diagrams and atomic structures of critical step through the CO pathways for urea formation on Mn@C₂N.

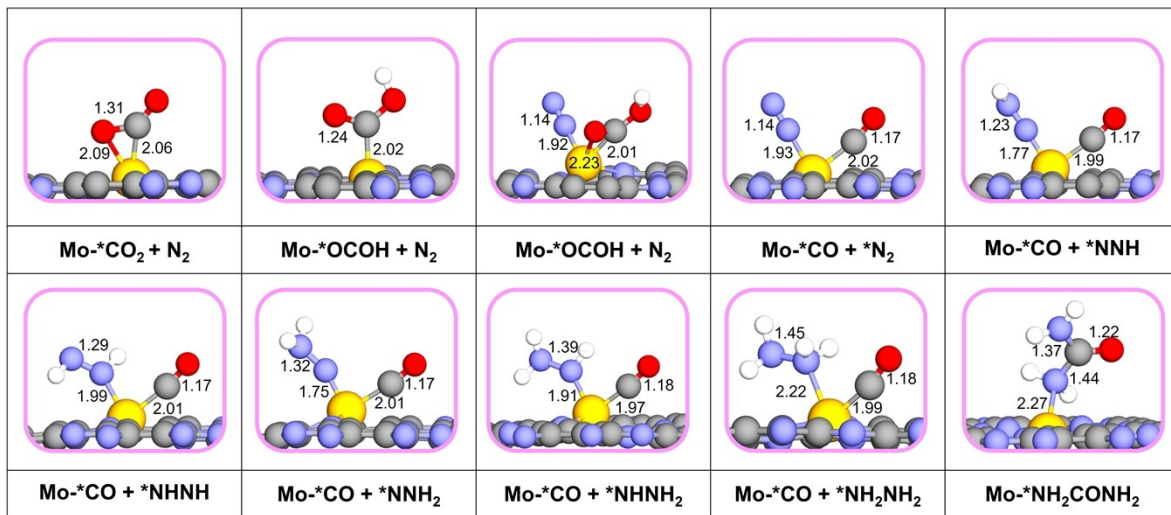
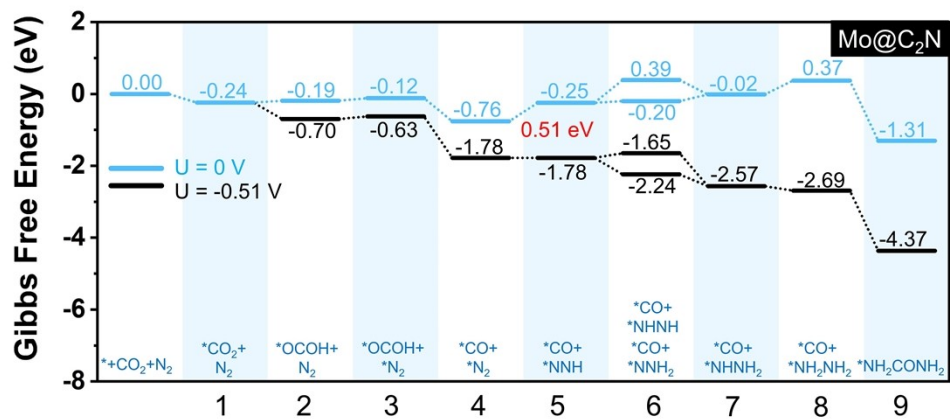


Figure 28 – Gibbs free energy diagrams and atomic structures of critical step through the CO pathways for urea formation on Mo@C₂N.

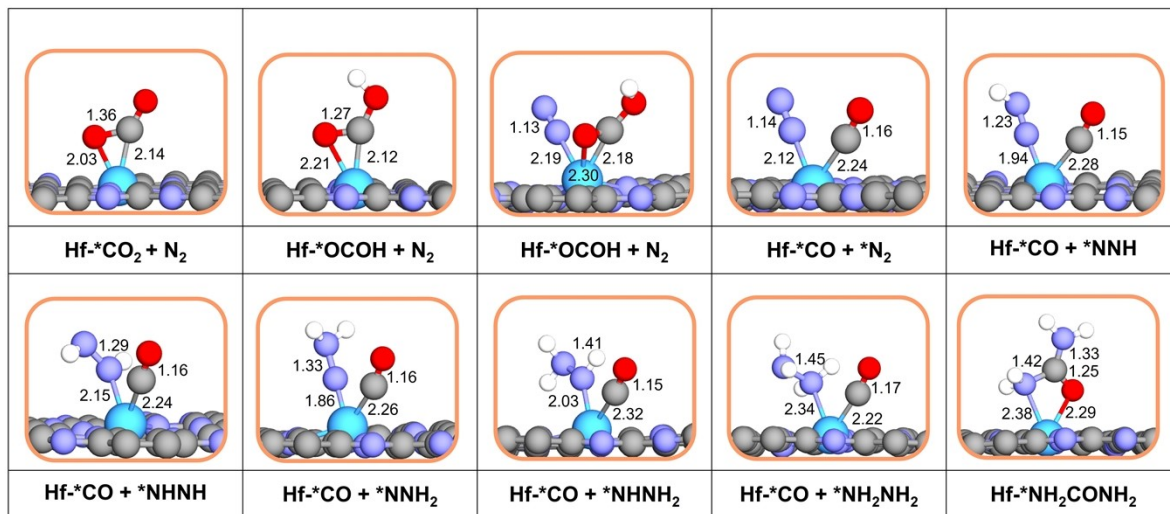
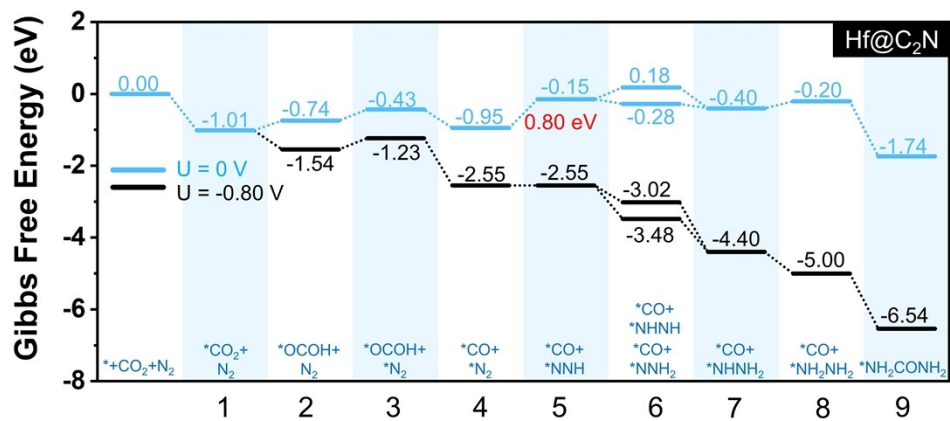


Figure29 – Gibbs free energy diagrams and atomic structures of critical step through the CO pathways for urea formation on Hf@C₂N.

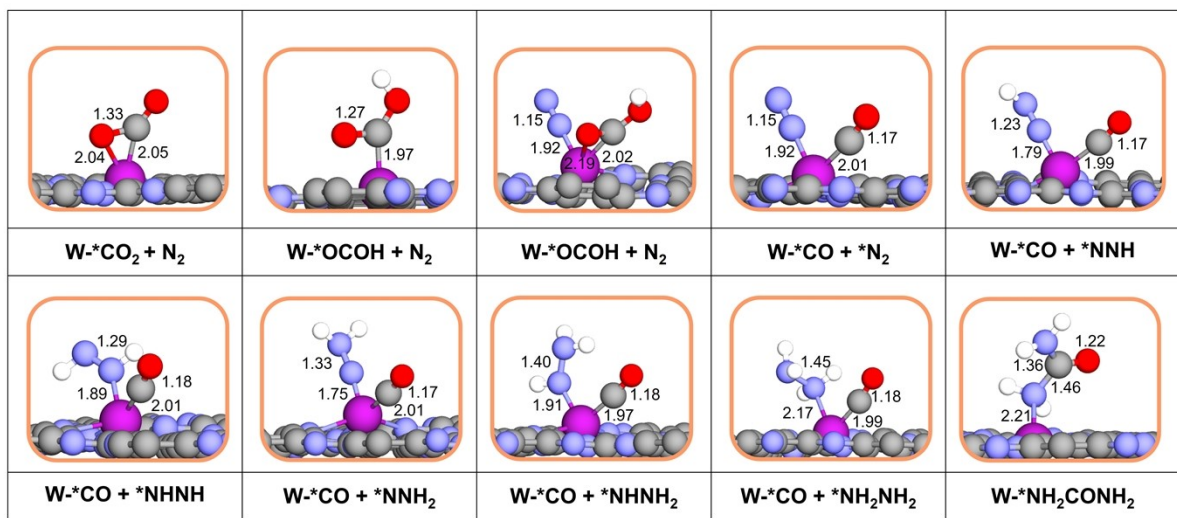
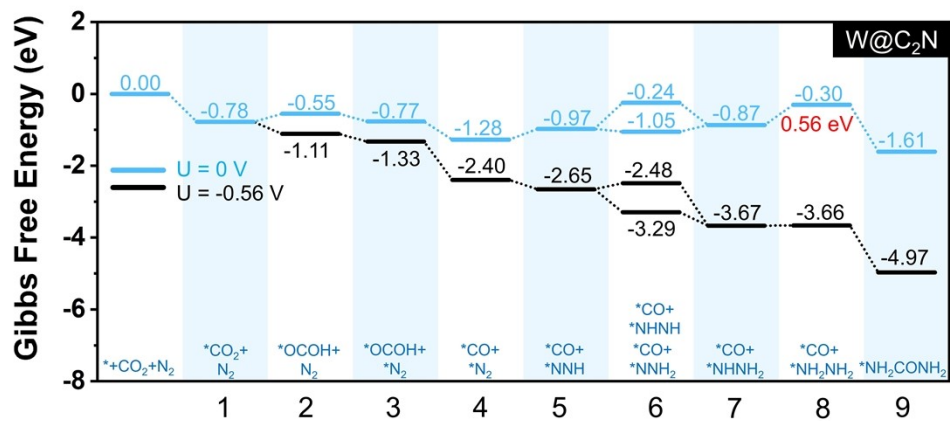


Figure30 – Gibbs free energy diagrams and atomic structures of critical step through the CO pathways for urea formation on $\text{W}@\text{C}_2\text{N}$.

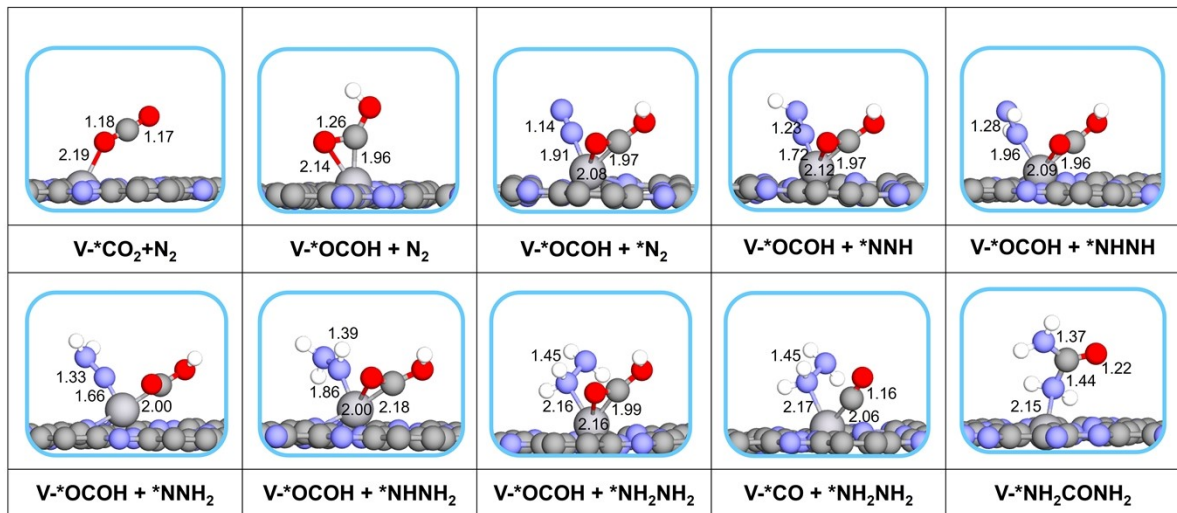
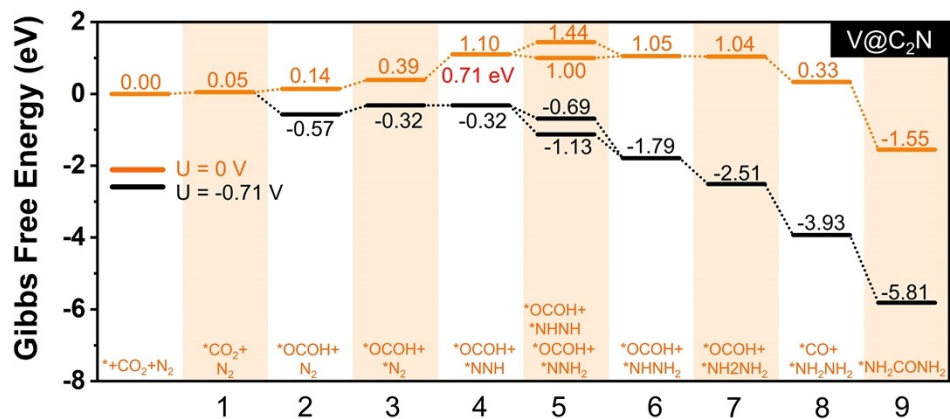


Figure31 – Gibbs free energy diagrams and atomic structures of critical step through the OCOH pathways for urea formation on V@C₂N.

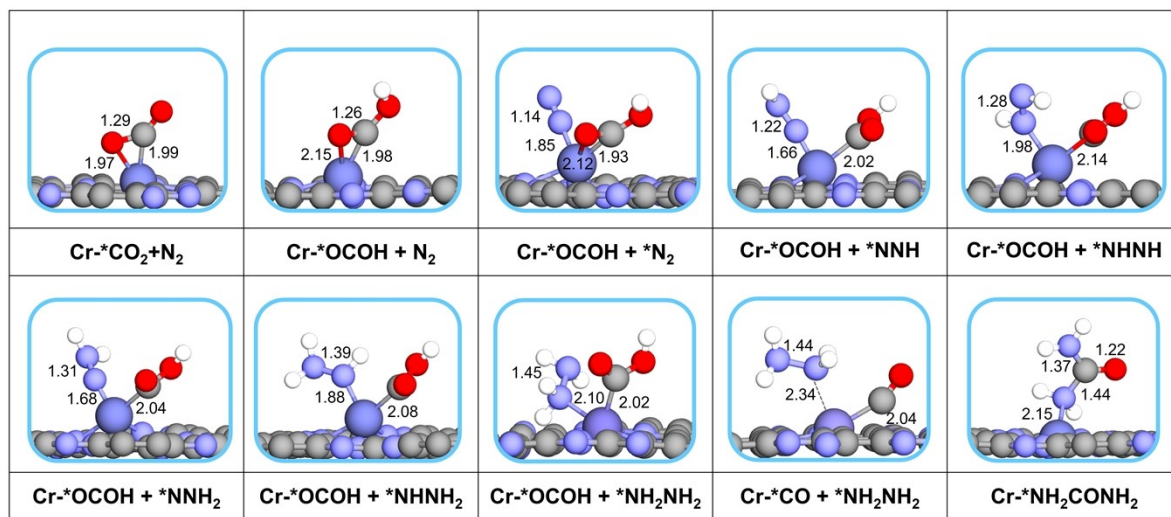
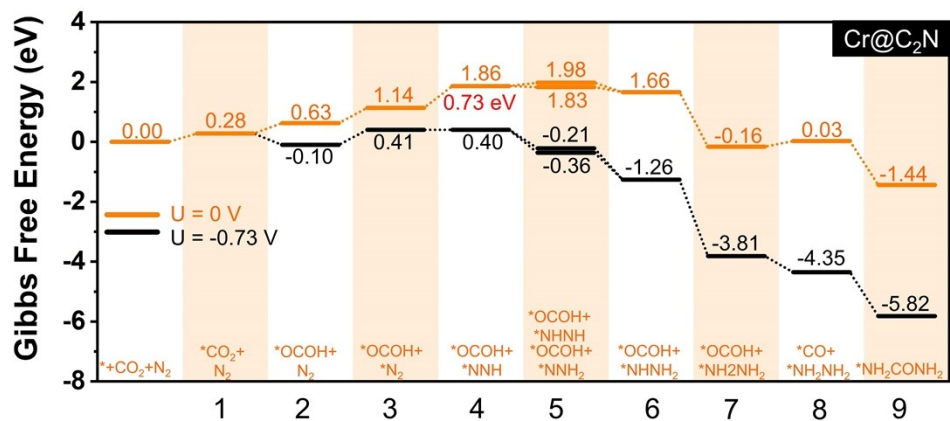


Figure32 – Gibbs free energy diagrams and atomic structures of critical step through the OCOH pathways for urea formation on Cr@C₂N.

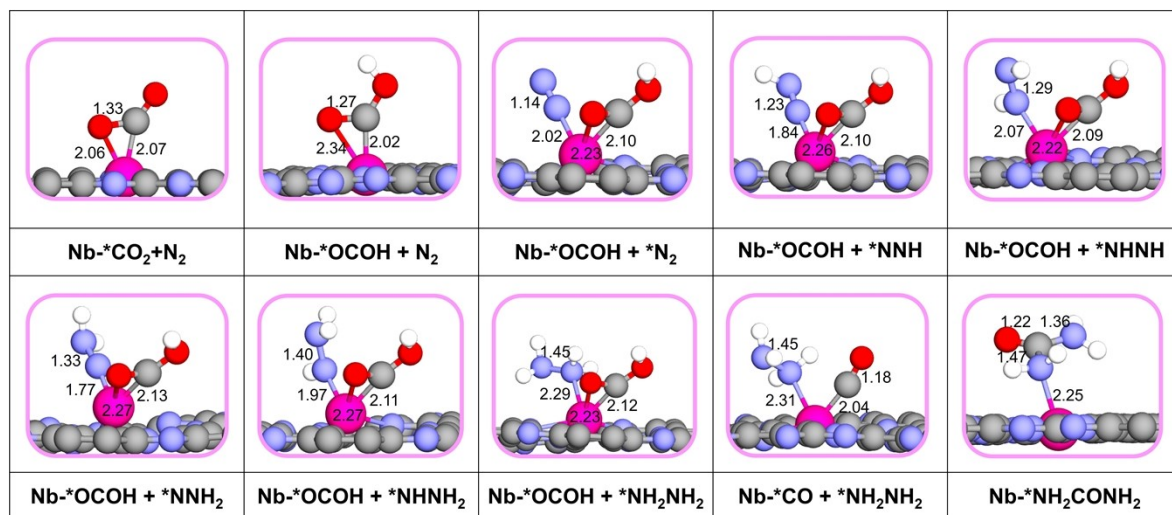
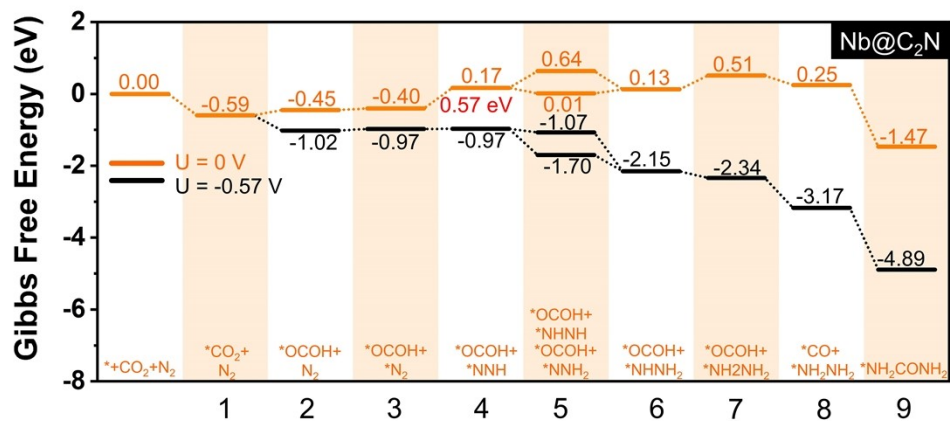


Figure33 – Gibbs free energy diagrams and atomic structures of critical step through the OCOH pathways for urea formation on Nb@C₂N.

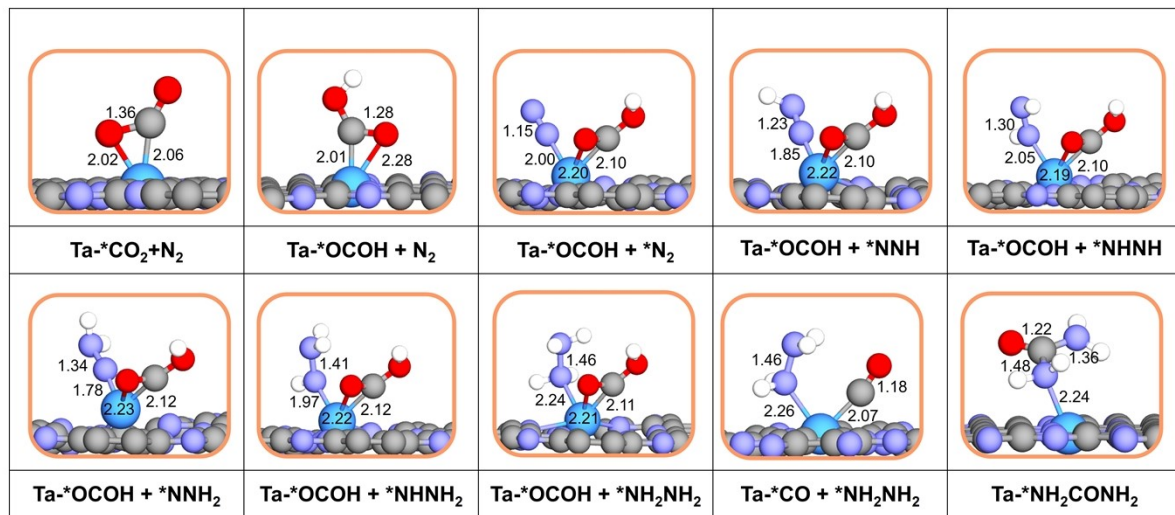
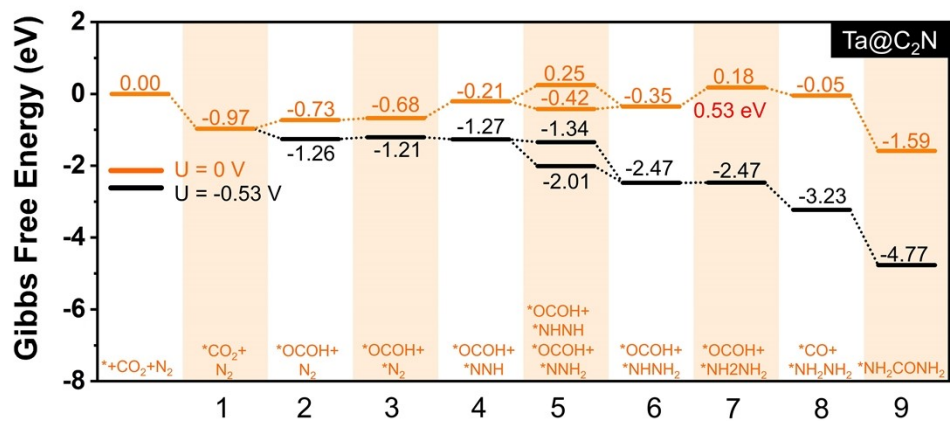


Figure34 – Gibbs free energy diagrams and atomic structures of critical step through the OCOH pathways for urea formation on Ta@C₂N.

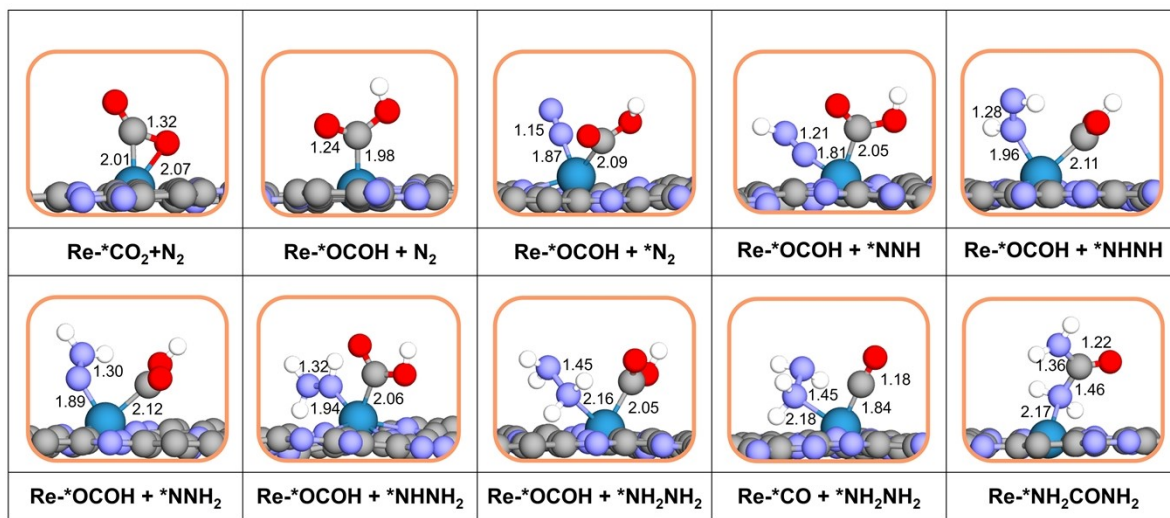
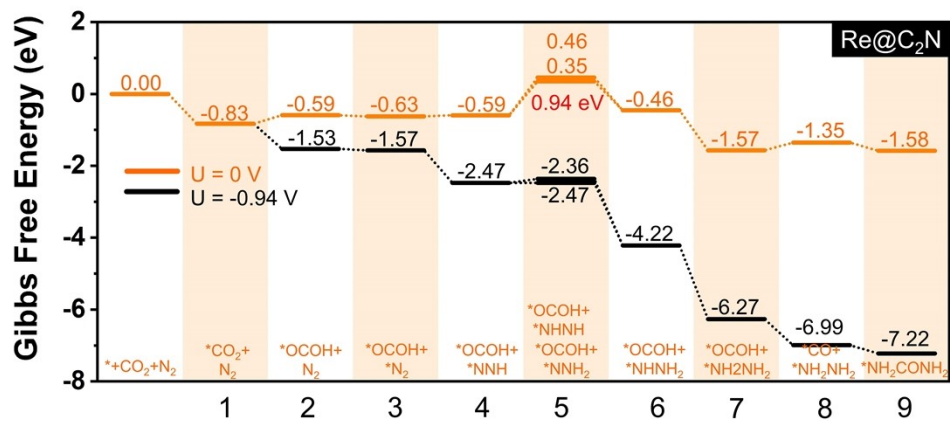


Figure35 – Gibbs free energy diagrams and atomic structures of critical step through the OCOH pathways for urea formation on Re@C₂N.

Table S2 The limiting potential of urea production (U_L) on the screened M@C₂N surface (M; Ti, V, Cr, Mn, Nb, Mo, Ru, Hf, Ta, W, and Re).

Catalysts	Urea production		
	Pathway	Limiting step	U_L
Ti@C ₂ N	CO	*CO + *N ₂ → *CO + *NNH	-0.85
Mn@C ₂ N	CO	*CO + *N ₂ → *CO + *NNH	-0.73
Mo@C ₂ N	CO	*CO + *N ₂ → *CO + *NNH	-0.51
Hf@C ₂ N	CO	*CO + *N ₂ → *CO + *NNH	-0.80
W@C ₂ N	CO	*CO + *NHNH ₂ → *CO + *NH ₂ NH ₂	-0.56
V@C ₂ N	OCOH	*OCOH + *N ₂ → *OCOH + *NNH	-0.71
Cr@C ₂ N	OCOH	*OCOH + *N ₂ → *OCOH + *NNH	-0.73
Nb@C ₂ N	OCOH	*OCOH + *N ₂ → *OCOH + *NNH	-0.57
Ta@C ₂ N	OCOH	*OCOH + *NHNH ₂ → *OCOH + *NH ₂ NH ₂	-0.53
Re@C ₂ N	OCOH	*OCOH + *NHNH ₂ → *OCOH + *NH ₂ NH ₂	-0.94
Ti@C ₂ N	CO ₂	*CO ₂ + *NHNH ₂ → *CO + *NH ₂ NH ₂	-0.90
V@C ₂ N	CO ₂	*CO ₂ + *NHNH ₂ → *CO + *NH ₂ NH ₂	-0.60
Cr@C ₂ N	CO ₂	*CO ₂ + *NHNH ₂ → *CO + *NH ₂ NH ₂	-0.87
Zr@C ₂ N	CO ₂	*CO ₂ + *NHNH ₂ → *CO + *NH ₂ NH ₂	-0.64
Nb@C ₂ N	CO ₂	*CO ₂ + *N ₂ → *CO ₂ + *NNH	-0.50
Hf@C ₂ N	CO ₂	*CO ₂ + *NHNH ₂ → *CO + *NH ₂ NH ₂	-0.78
Ta@C ₂ N	CO ₂	*CO ₂ + *NHNH ₂ → *CO + *NH ₂ NH ₂	-0.62
W@C ₂ N	CO ₂	*CO ₂ + *N ₂ → *CO ₂ + *NNH	-0.60
Re@C ₂ N	CO ₂	*CO ₂ + *N ₂ → *CO ₂ + *NNH	-0.51

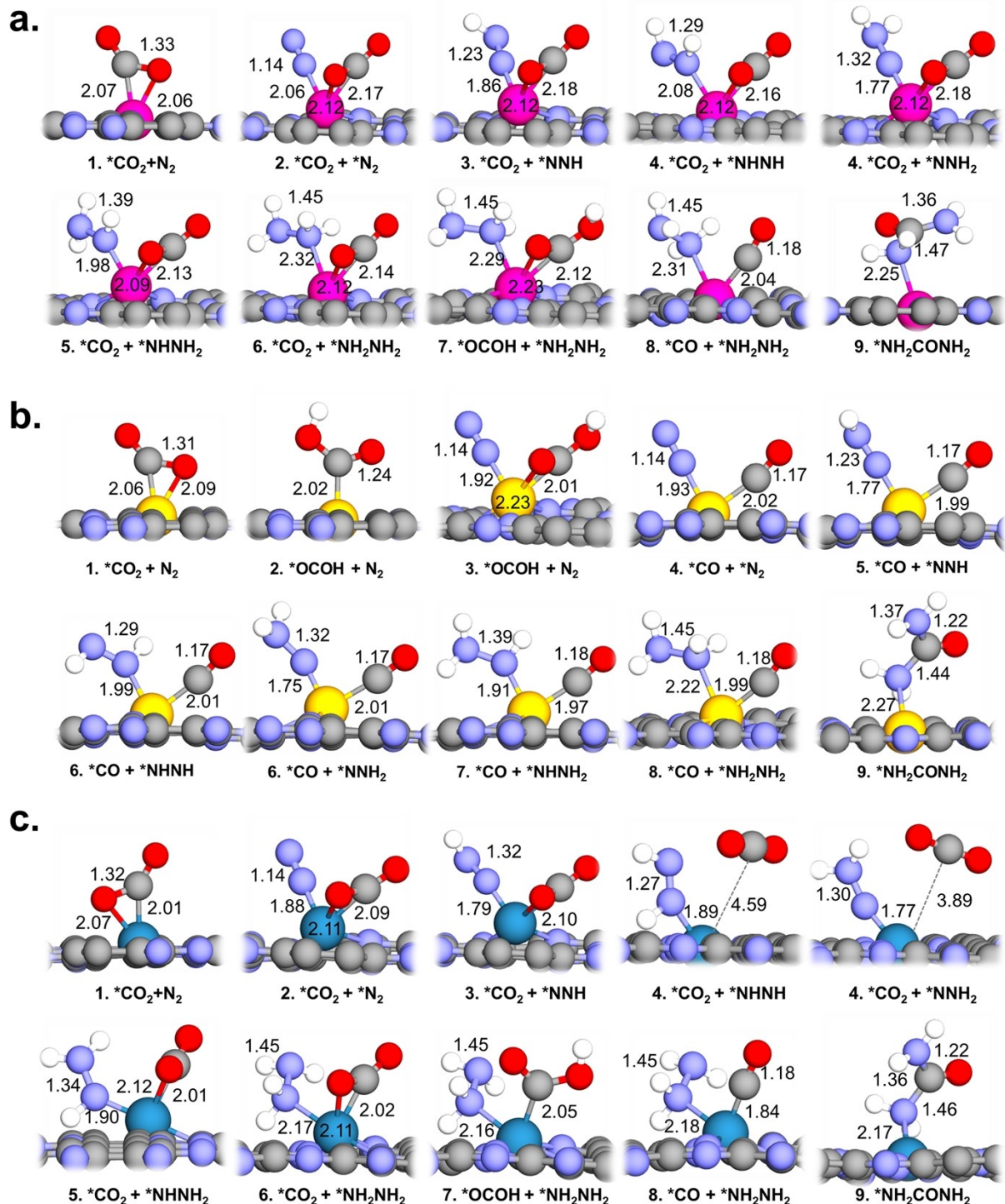


Figure36 – The geometrical structures of (a.) Nb@C₂N, (b.) Mo@C₂N and (c.) Re@C₂N catalysts

Table R3 Gibbs free energy (G, eV) and Nb magnetization values (μ_B) of the intermediates in the $*\text{CO}_2 + *\text{N}_2 \rightarrow *\text{CO}_2 + *\text{NNH}$ step on Nb@C₂N at different U values.

	U		PBE0
	U = 0.00	U = 4.0 ^{6, 7}	
$G_{*\text{CO}_2 + *\text{N}_2}$	-0.55	0.14	-0.56
$G_{*\text{CO}_2 + *\text{NNH}}$	-0.05	1.08	-0.06
ΔG_{PDS}	0.50	0.95	0.50
Nb magnetization			
*	1.3373	2.0468	1.3368
$*\text{CO}_2 + *\text{N}_2$	0.9952	1.0032	0.9952
$*\text{CO}_2 + *\text{NNH}$	0.0000	0.0000	0.0000

Table R4 Gibbs free energy (G, eV) and Mo magnetization values (μ_B) of the intermediates in the $*\text{CO} + *\text{N}_2 \rightarrow *\text{CO} + *\text{NNH}$ step on Mo@C₂N at different U values.

	U				PBE0
	U = 0.00	U = 2.30 ⁸	U = 4.38 ⁹	U = 8.60 ¹⁰	
$G_{*\text{CO}_2 + *\text{N}_2}$	-0.76	0.05	0.88	2.17	-0.76
$G_{*\text{CO}_2 + *\text{NNH}}$	-0.25	0.89	2.12	3.56	-0.26
ΔG_{PDS}	0.51	0.84	1.24	1.39	0.50
Mo magnetization					
*	2.2399	2.2396	3.1396	3.3772	2.2399
$*\text{CO} + *\text{N}_2$	1.2689	1.5954	1.7286	1.7285	1.2695
$*\text{CO} + *\text{NNH}$	0.0000	0.0000	0.0000	1.4992	0.0001

Table R5 Gibbs free energy (G, eV) and Re magnetization values (μ_B) of the intermediates in the $*\text{CO}_2 + *\text{N}_2 \rightarrow *\text{CO}_2 + *\text{NNH}$ step on Re@C₂N at different U values.

	U		PBE0
	U = 0.00	U = 2.3 ^{11, 12}	
$G_{*\text{CO}_2 + *\text{N}_2}$	-0.87	0.01	-1.11
$G_{*\text{CO}_2 + *\text{NNH}}$	-0.44	0.75	-0.70
ΔG_{PDS}	0.43	0.74	0.41
Re magnetization			
*	2.7685	2.0122	2.7680
$*\text{CO}_2 + *\text{N}_2$	0.0000	0.0005	0.0008
$*\text{CO}_2 + *\text{NNH}$	0.0000	0.0001	0.0001

Table R6 Gibbs free energy (G, eV) of the intermediates in the $^*\text{CO}_2/\text{CO} + ^*\text{N}_2 \rightarrow ^*\text{CO}_2/\text{CO} + ^*\text{NNH}$ step on Nb@C₂N with and without VASPsol calculation.

	Nb		Mo		Re	
	VASP	VASPsol	VASP	VASPsol	VASP	VASPsol 1
$G_{^*\text{CO}_2/\text{CO} + ^*\text{N}_2}$	-0.55	-0.48	-0.76	-0.80	-0.87	-0.95
$G_{^*\text{CO}_2/\text{CO} + ^*\text{NNH}}$	-0.05	0.00	-0.25	-0.28	-0.44	-0.39
ΔG_{PDS}	0.50	0.48	0.51	0.52	0.43	0.57

Table S7. Specific values of different features are included in the descriptor Φ .

Elements	N_d	χ	Φ	Elements	N_d	χ	Φ
Sc	1	1.36	3.66	Rh	8	2.18	23.14
Ti	2	1.54	6.88	Pd	10	2.2	28.79
V	3	1.63	10.04	Ag	10	1.93	30.74
Cr	5	1.66	16.57	Hf	2	1.32	7.43
Mn	5	1.55	17.15	Ta	3	1.51	10.43
Fe	6	1.83	18.94	W	4	2.36	11.12
Co	7	1.88	21.80	Re	5	1.93	15.37
Ni	8	1.92	24.66	Os	6	2.18	17.36
Cu	10	1.9	30.98	Ir	7	2.2	20.16
Y	1	1.22	3.87	Pt	9	2.28	25.46
Zr	2	1.33	7.41	Au	10	2.54	26.80
Nb	4	1.59	13.55	N	N/A	3.04	N/A
Mo	5	2.16	14.53	Substrate [#]	N/A	18.24	N/A
Ru	7	2.2	20.16				

[#] $c_{sub} = nc_N$, where n are 6 in the M@C₂N. Therefore, Φ can be simplified as

$$\Phi = \frac{N_d}{\sqrt{c_M / (6 \times 3.04)}} = \frac{N_d}{\sqrt{c_M / 18.24}}$$

Table S8. Specific values of different features are included in the descriptor φ .

Elements	N _d	χ	χ_{avg}	φ	Elements	N _d	χ	χ_{avg}	φ
Sc	1	1.36	4.27	1.40	Rh	8	2.18	4.40	11.59
Ti	2	1.54	4.30	2.83	Pd	10	2.2	4.41	14.50
V	3	1.63	4.31	4.25	Ag	10	1.93	4.36	14.35
Cr	5	1.66	4.32	7.10	Hf	2	1.32	4.26	2.80
Mn	5	1.55	4.30	7.07	Ta	3	1.51	4.29	4.24
Fe	6	1.83	4.35	8.58	W	4	2.36	4.43	5.83
Co	7	1.88	4.35	10.02	Re	5	1.93	4.36	7.17
Ni	8	1.92	4.36	11.47	Os	6	2.18	4.40	8.69
Cu	10	1.9	4.36	14.33	Ir	7	2.2	4.41	10.15
Y	1	1.22	4.24	1.40	Pt	9	2.28	4.42	13.09
Zr	2	1.33	4.26	2.80	Au	10	2.54	4.46	14.68
Nb	4	1.59	4.31	5.66	N	N/A	3.04	N/A	N/A
Mo	5	2.16	4.40	7.24	Substrate [#]	N/A	18.24	N/A	N/A
Ru	7	2.2	4.41	10.15					

Table S9. Values of descriptor Φ and U_L of PDS for urea production over reported electrocatalysts.

Electrocatalysts		Φ	U_L (V)
	Sc	3.66	-1.02
	Ti	6.88	-0.85
	V	10.04	-0.60
	Cr	16.57	-0.73
	Mn	17.15	-0.73
	Fe	18.94	-1.07
	Co	21.80	-1.32
	Ni	24.66	-1.14
	Cu	30.98	-1.49
	Y	3.87	-1.07
	Zr	7.41	-0.64
M@C ₂ N	Nb	13.55	-0.50
	Mo	14.53	-0.51
	Ru	20.16	-1.07
	Rh	23.14	-1.20
	Pd	28.79	-1.31
	Hf	7.43	-0.78
	Ta	10.43	-0.62
	W	11.12	-0.56
	Re	15.37	-0.51
	Os	17.36	-0.88
	Ir	20.16	-1.21
	Pt	25.46	-0.98
	Sc	3.24	-0.93
	Ti	6.09	-0.74
M ₂ @C ₃ N ₄ ¹³	V	8.88	-0.74
	Cr	14.67	-1.54
	Mn	15.18	-1.03

	Fe	16.76	-1.80
	Co	19.30	-1.86
	Ni	21.82	-2.67
	Cu	27.42	-3.41
	Zn	29.42	-3.35
	Y	3.42	-1.90
	Zr	6.55	-0.76
	Nb	11.99	-0.75
	Mo	12.86	-1.31
	Tc	13.67	-1.03
	Ru	17.84	-1.54
	Rh	20.48	-1.69
	Pd	25.48	-2.26
	Ag	27.21	-3.97
	Cd	29.07	-3.08
	Hf	6.58	-1.14
	Ta	9.23	-1.19
	W	9.84	-0.75
	Re	13.60	-1.51
	Os	15.36	-1.04
	Ir	17.84	-1.29
	Pt	22.53	-1.33
	Au	23.72	-3.07
M/p-BN ¹⁴	Fe	26.45	-0.63
	Co	30.44	-0.66
M-B@C ₂ N ¹⁵	Sc	3.56	-0.74
	Ti	6.69	-0.76
	V	9.76	-0.81
	Cr	16.11	-0.81
	Mn	16.68	-1.80
	Fe	18.42	-1.15

Co	21.20	-1.07
Ni	23.97	-1.72
Cu	30.12	-1.47
Zr	7.20	-0.62
Nb	13.17	-0.54
Mo	14.13	-0.53
Ru	19.60	-0.88
Rh	22.50	-1.39
Pd	27.99	-1.65
Ag	29.89	-2.06
PdCu ¹⁶	19.76	-0.64
Mo ₂ B ₂ ¹⁷	19.58	-0.49
Ti ₂ B ₂ ¹⁷	8.92	-0.65
Cr ₂ B ₂ ¹⁷	21.65	-0.52
V ₂ N ₆ C ¹⁸	19.25	-0.59
CuB ₁₂ ¹⁹	35.90	-0.23
CuPc ²⁰	48.52	-1.67
MoP(111) ²¹	28.48	-0.27

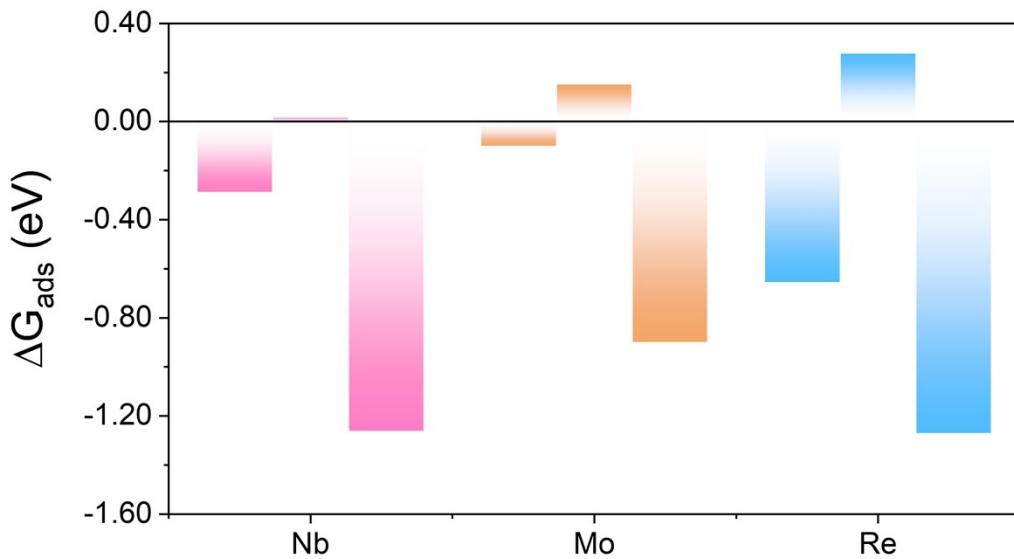


Figure37 – Gibbs free energy adsorption for H^+ , H_2O , and N_2 on $\text{Nb}@\text{C}_2\text{N}$, $\text{Mo}@\text{C}_2\text{N}$, and $\text{Re}@\text{C}_2\text{N}$ catalysts

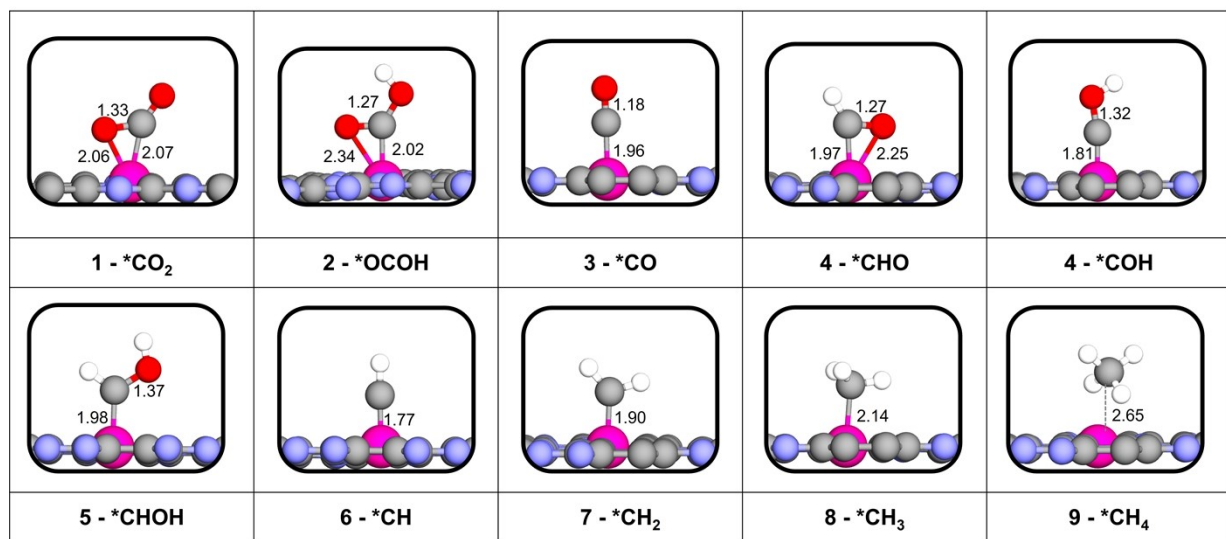
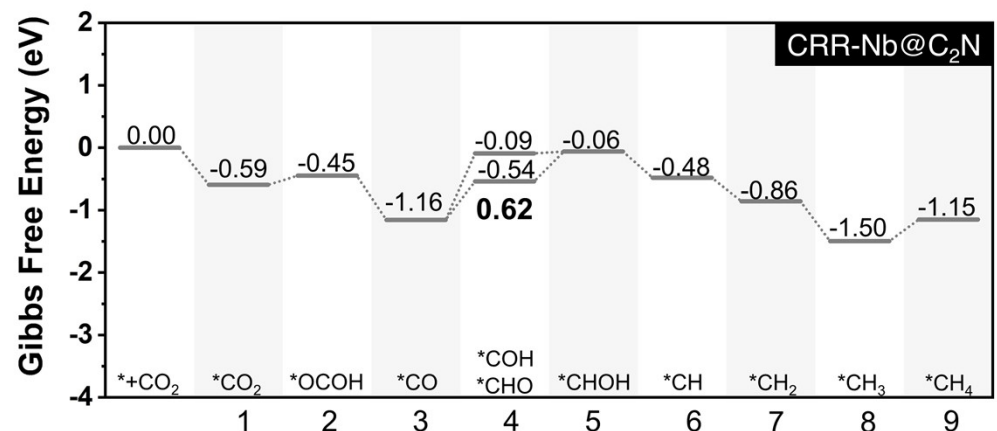


Figure38 – Gibbs free energy diagrams and atomic structures of CRR on Nb@C₂N catalysts

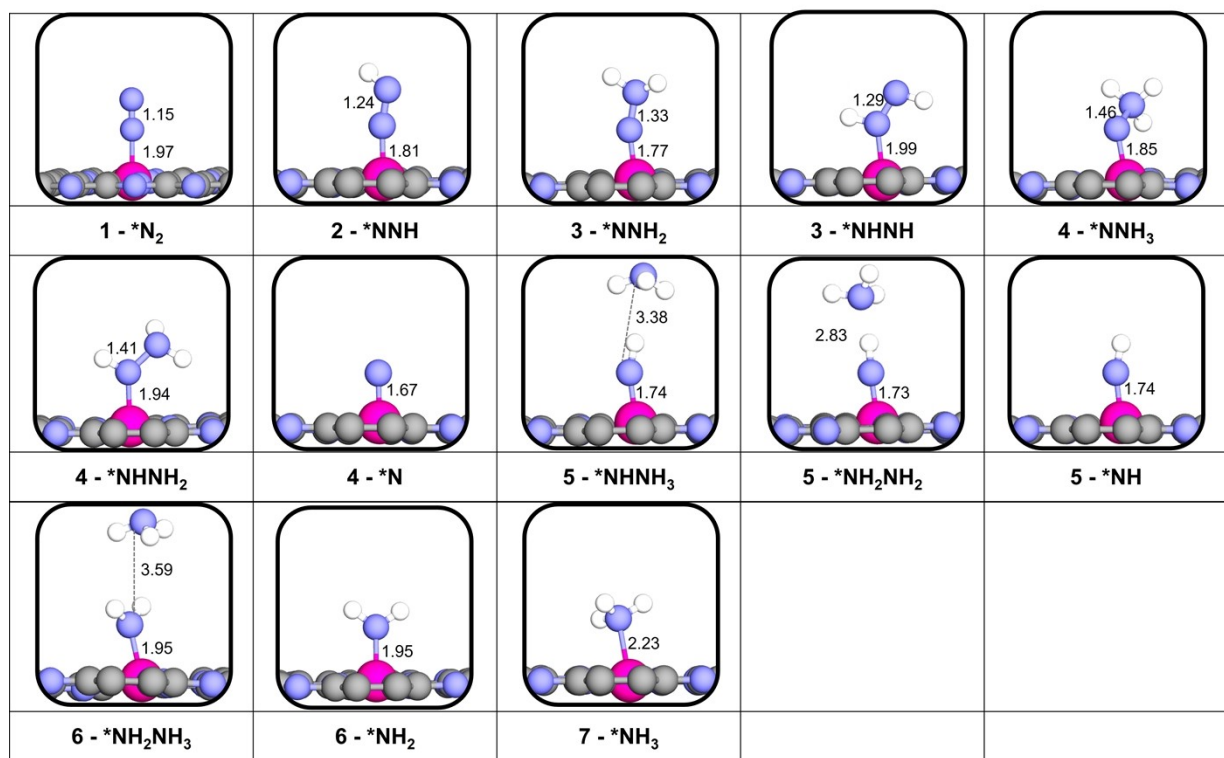
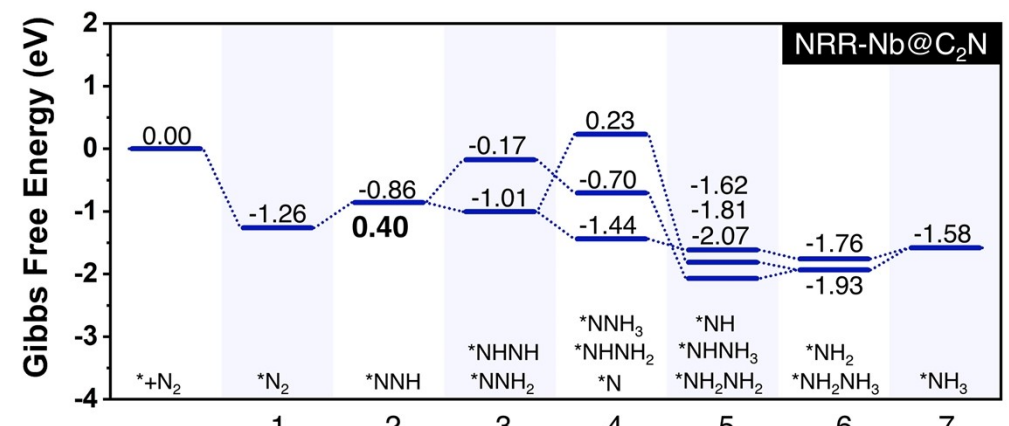


Figure39 – Gibbs free energy diagrams and atomic structures of NRR on Nb@C₂N catalysts

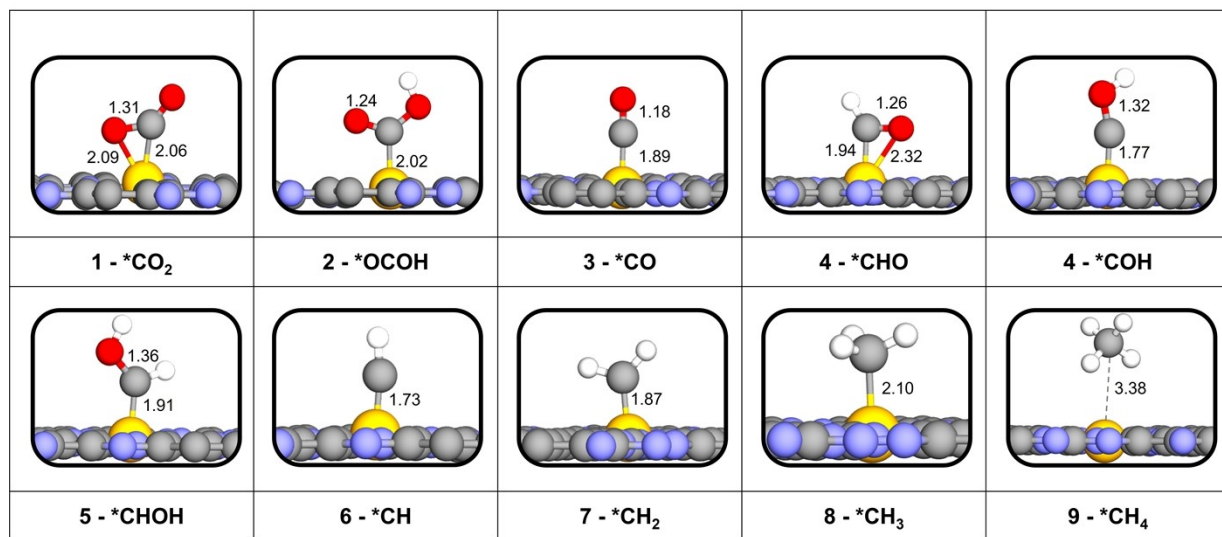
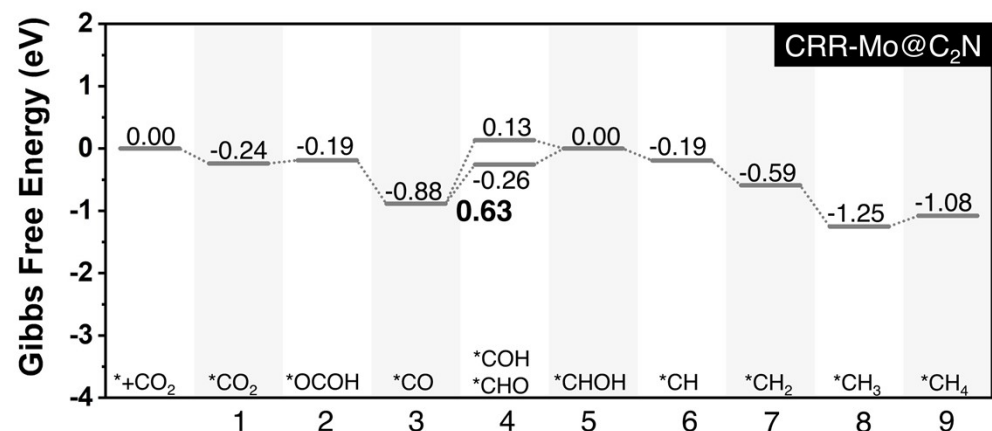


Figure40 – Gibbs free energy diagrams and atomic structures of CRR on Mo@C₂N catalysts

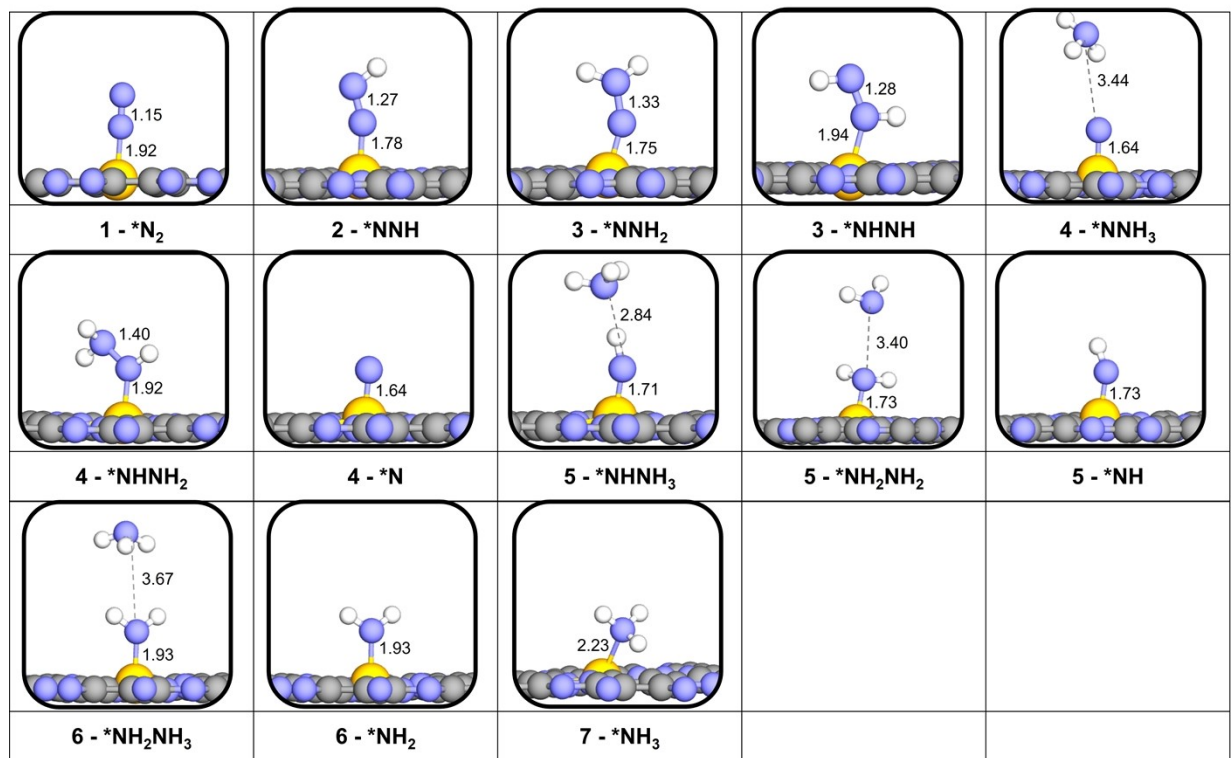
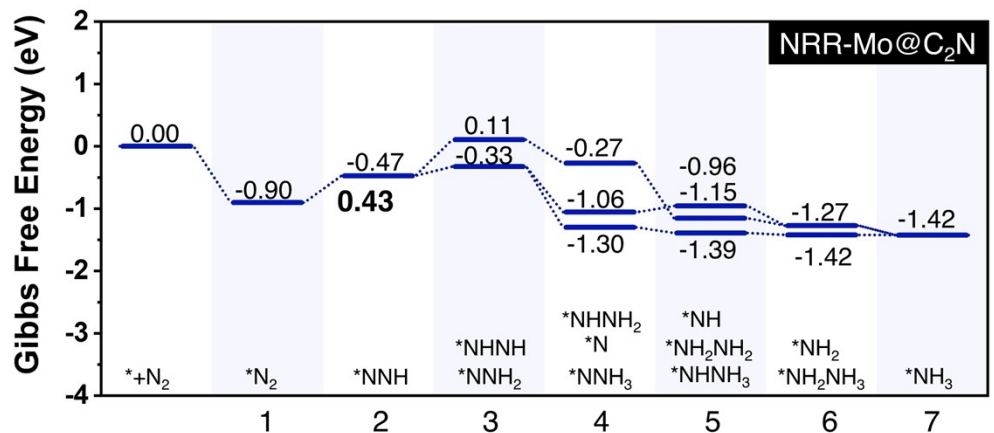


Figure41 – Gibbs free energy diagrams and atomic structures of NRR on Mo@C₂N catalysts

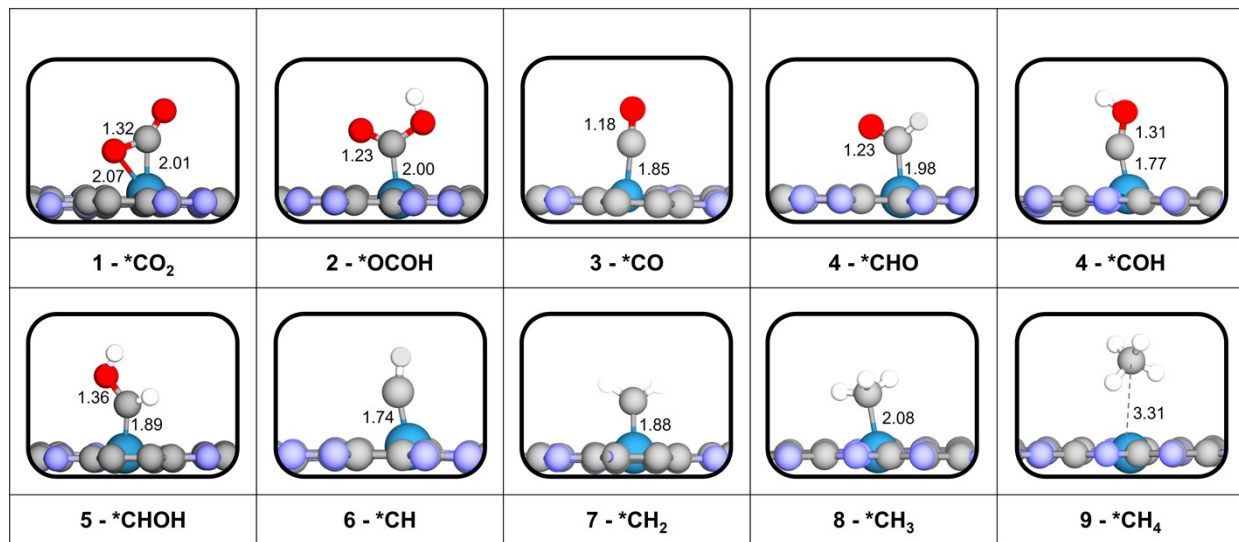
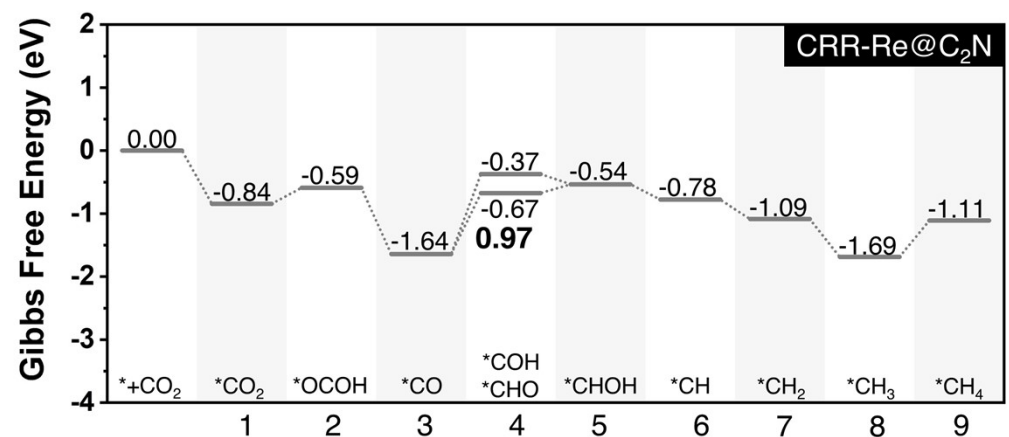


Figure42 – Gibbs free energy diagrams and atomic structures of CRR on Re@C₂N catalysts

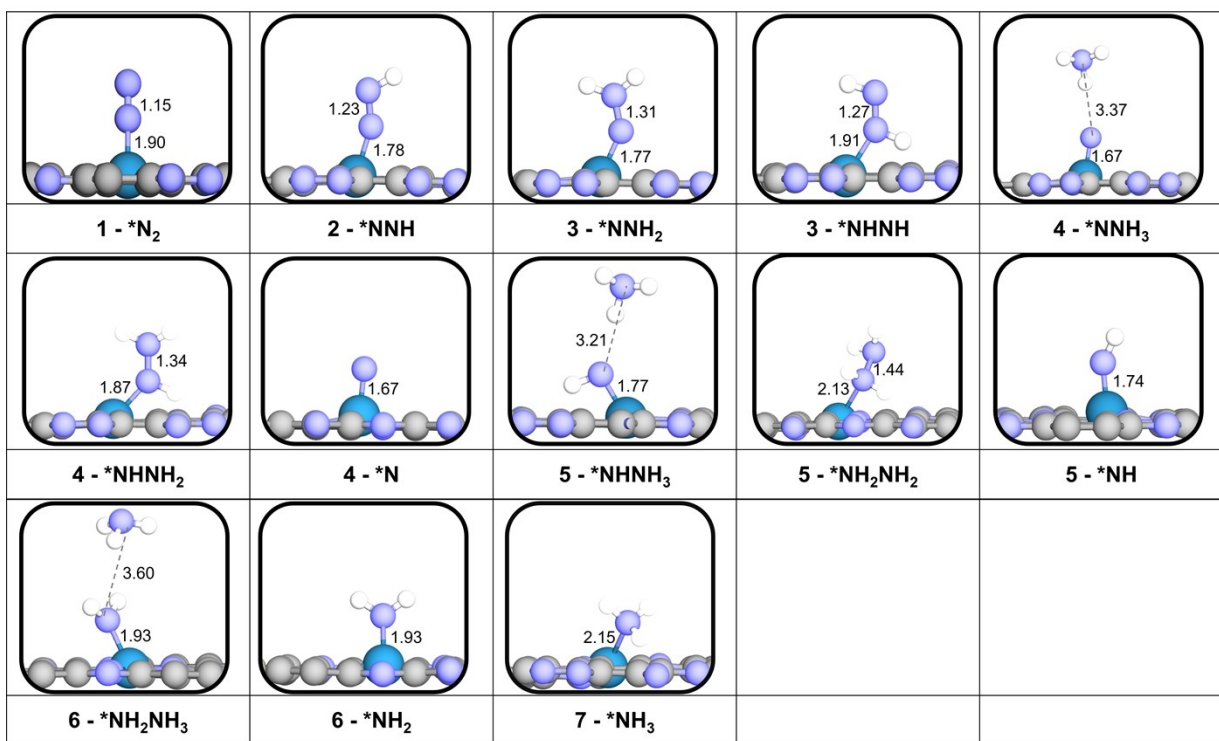
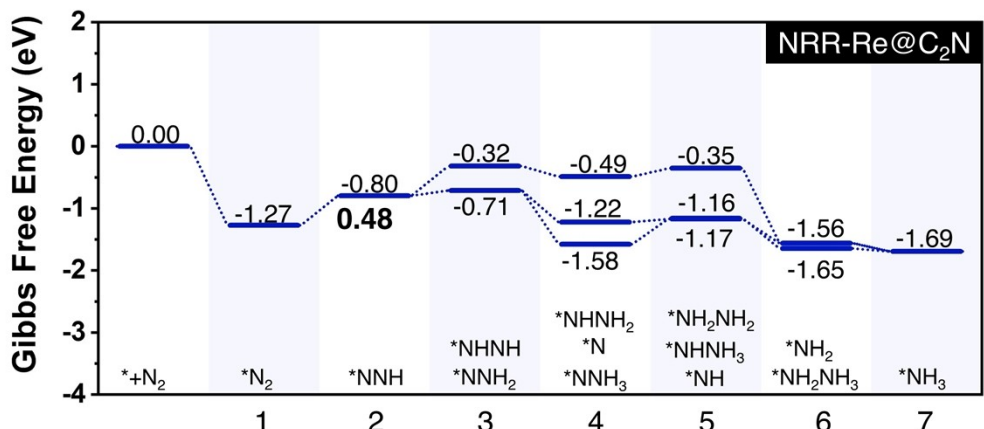


Figure43 – Gibbs free energy diagrams and atomic structures of NRR on Re@C₂N catalysts

References

1. X. Wang, N. Zhang, H. Shang, H. Duan, Z. Sun, L. Zhang, Y. Lei, X. Luo, L. Zhang and B. Zhang, *Nature Communications*, 2025, **16**, 470.
2. L.-Z. Yu, X.-W. Zhang, F. Wang, J. Xu and B. Xue, *Applied Catalysis A: General*, 2024, **678**, 119729.
3. F. Li, H. Du, T. Chen, Q. Zhu and Z. Yu, *International Journal of Applied Ceramic Technology*, 2023, **20**, 1090-1102.
4. Z. Chen, S. Wang, H. Zhou and S. Zeng, *RSC Advances*, 2025, **15**, 7869-7875.
5. C. Shen, K. Sun, R. Zou, Q. Wu, D. Mei and C.-j. Liu, *ACS Catalysis*, 2022, **12**, 12658-12669.
6. H. H. Nahm and C. Park, *Physical Review B—Condensed Matter and Materials Physics*, 2008, **78**, 184108.
7. D. Ren, H. Li and X. Cheng, *Solid State Communications*, 2015, **223**, 54-59.
8. D. Misra, G. Di Liberto and G. Pacchioni, *Physical Chemistry Chemical Physics*, 2024, **26**, 10746-10756.
9. M. Wang and A. Navrotsky, *Solid State Ionics*, 2004, **166**, 167-173.
10. S. Lutfalla, V. Shapovalov and A. T. Bell, *Journal of chemical theory and computation*, 2011, **7**, 2218-2223.
11. M. Cococcioni and S. De Gironcoli, *Physical Review B—Condensed Matter and Materials Physics*, 2005, **71**, 035105.
12. M. Wierzbowska, *Journal of Physics: Condensed Matter*, 2012, **24**, 126002.
13. C. Zhu, M. Wang, C. Wen, M. Zhang, Y. Geng, G. Zhu and Z. Su, *Advanced Science*, 2022, **9**, 2105697.
14. L. Kong, D. Jiao, Z. Wang, Y. Liu, Y. Shang, L. Yin, Q. Cai and J. Zhao, *Chemical Engineering Journal*, 2023, **451**, 138885.
15. N. Yodsin, P. Mano, K. Takahashi and S. Namuangruk, *ChemCatChem*, 2024, **16**, e202400304.
16. C. Chen, X. Zhu, X. Wen, Y. Zhou, L. Zhou, H. Li, L. Tao, Q. Li, S. Du and T. Liu, *Nature chemistry*, 2020, **12**, 717-724.
17. X. Zhu, X. Zhou, Y. Jing and Y. Li, *Nature Communications*, 2021, **12**, 4080.
18. Z. Zhang and L. Guo, *Dalton Transactions*, 2021, **50**, 11158-11166.
19. C. Zhu, C. Wen, M. Wang, M. Zhang, Y. Geng and Z. Su, *Chemical Science*, 2022, **13**, 1342-1354.
20. J. Mukherjee, S. Paul, A. Adalder, S. Kapse, R. Thapa, S. Mandal, B. Ghorai, S. Sarkar and U. K. Ghorai, *Advanced Functional Materials*, 2022, **32**, 2200882.
21. D. Jiao, Y. Dong, X. Cui, Q. Cai, C. R. Cabrera, J. Zhao and Z. Chen, *Journal of Materials Chemistry A*, 2023, **11**, 232-240.